Summer 2004

Spectrum control and iterative coding for high capacity multiband OFDM

Divaydeep Sikri
New Jersey Institute of Technology

ABSTRACT

SPECTRUM CONTROL AND ITERATIVE CODING FOR HIGH CAPACITY MULTIBAND OFDM

by
Divaydeep Sikri

The emergence of Multiband Orthogonal Frequency Division Modulation (MB-OFDM) as an ultra-wideband (UWB) technology injected new optimism in the market through realistic commercial implementation, while keeping promise of high data rates intact. However, it has also brought with it host of issues, some of which are addressed in this thesis.

The thesis primarily focuses on the two issues of spectrum control and user capacity for the system currently proposed by the Multiband OFDM Alliance (MBOA). By showing that line spectra are still an issue for new modulation scheme (MB-OFDM), it proposes a mechanism of scrambling the data with an increased length linear feedback shift register (compared to the current proposal), a new set of seeds, and random phase reversion for the removal of line spectra. Following this, the thesis considers a technique for increasing the user capacity of the current MB-OFDM system to meet the needs of future wireless systems, through an adaptive multiuser synchronous coded transmission scheme. This involves real time iterative generation of user codes, which are generated over time and frequency leading to increased capacity. With the assumption of complete channel state information (CSI) at the receiver, an iterative MMSE algorithm is used which involves replacement of each user's signature with its normalized MMSE filter function allowing the overall Total Squared Correlation (TSC) of the system to decrease until the algorithm converges to a fixed set of signature vectors. This allows the system to

be overloaded and user's codes to be quasi-orthogonal. Simulation results show that for code of length nine (spread over three frequency bands and three time slots), ten users can be accommodated for a given QoS and with addition of single frequency sub-band which allows the code length to increase from nine to twelve (four frequency sub-bands and three time slots), fourteen users with nearly same QoS can be accommodated in the system. This communication is overlooked by a central controller with necessary functionalities to facilitate the process. The thesis essentially considers the uplink from transmitting devices to this central controller. Furthermore, analysis of this coded transmission in presence of interference is carried to display the robustness of this scheme through its adaptation by incorporating knowledge of existing Narrowband (NB) Interference for computing the codes. This allows operation of sub-band coexisting with NB interference without substantial degradation given reasonable interference energy (SIR=-10dB and -5dB considered). Finally, the thesis looks at design implementation and convergence issues related to code vector generation whereby, use of Lanczos algorithm is considered for simpler design and faster convergence. The algorithm can be either used to simplify design implementation by providing simplified solution to Weiner Hopf equation (without requiring inverse of correlation matrix) over Krylov subspace or can be used to expedite convergence by updating the signature sequence with eigenvector corresponding to the least eigenvalue of the signature correlation matrix through reduced rank eigen subspace search.

SPECTRUM CONTROL AND ITERATIVE CODING FOR HIGH CAPACITY MULTIBAND OFDM

by
Divaydeep Sikri

A Dissertation
Submitted to the Faculty of
New Jersey Institute of Technology
in Partial Fulfillment of the Requirements for the Degree of
Master of Science in Electrical Engineering

Department of Electrical and Computer Engineering

August 2004

APPROVAL PAGE

SPECTRUM CONTROL AND ITERATIVE CODING FOR HIGH CAPACITY MULTIBAND OFDM

Divaydeep Sikri

Dr. Alexander M. Haimovich, Dissertation Advisor — Date
Professor of Electrical and Computer Engineering, NJIT

Dr. Ali Abdi, Committee Member — Date
Assistant Professor of Electrical and Computer Engineering, NJIT

Dr. Samuel Mo, Committee Member — Date
Senior Scientist, Panasonic International Telecomm. & Networking Lab, Princeton, NJ

BIOGRAPHICAL SKETCH

Author: Divaydeep Sikri

Degree: Master of Science

Date: August 2004

Undergraduate and Graduate Education:

- Master of Science in Electrical Engineering,
  New Jersey Institute of Technology, Newark, NJ, 2004

- Bachelor of Science in Electrical Engineering,
  Netaji Subhas Institute of Technology, New Delhi, India, 2002

Major: Electrical Engineering

Patents:

Divaydeep Sikri, Alexander M. Haimovich, Samuel M. Mo and Alexander Gelman
"Ultra Wideband scrambler for reducing power spectral density,"
Patent number 60/535,392, pending approval.

Divaydeep Sikri, Alexander M. Haimovich, Samuel M. Mo and Alexander Gelman
"Flexible Code-Assignment for Enhanced User Capacity Multiband OFDM ,"
Pending approval.

To my beloved family

ACKNOWLEDGMENT

I convey my sincere thanks to my thesis advisor, Dr. Alexander Haimovich, whose constant guidance, helpful suggestions and reassurance helped me, carry out the thesis work satisfactorily. I would also like to thank Dr. Samuel Mo for providing the necessary resources to carry out the work and also for being an integral part of the committee. Special thanks to Dr. Ali Abdi, for actively participating in the committee.

I want to take this opportunity to acknowledge the immense help, encouragement and support I have received from my family, my mother, my father and my younger sister. I am thankful to every little piece of advice and concern they have spoken over the years.

Words are inadequate to express my thanks to all my friends whose names have not been mentioned but have helped me directly or indirectly in my endeavor.

TABLE OF CONTENTS

Chapter	Page
1 INTRODUCTION	1
1.1 Bluetooth and Wireless Personal Area Network	1
1.2 UltraWideband	4
1.2.1 Single Band	7
1.2.2 Multiband	7
2 POWER SPECTRAL DENSITY OF CYCLOSTATIONARY PROCESSES	14
2.1 Cyclostationary Processes	14
2.2 PSD of Linearly Modulated Signals	16
3 BASEBAND WHITENING OF MULTIBAND-OFDM UWB SIGNALS	19
3.1 Current Implementation in Wireless Systems	20
3.1.1 PSD of MB-OFDM UWB	20
3.1.2 Current Scrambler in MB-OFDM Proposal to IEEE 802.15.3a	23
3.2 Proposed Mechanism	23
3.2.1 Phase Reversion to Minimize PSD of MB-OFDM UWB Signals	23
3.3 Scrambler Design for MB-OFDM UWB System to IEEE 802.15.3a	29
3.3.1 New Four Seeds for Scramblers	29
3.3.2 LFSR-28 for Scrambler	30
3.3.3 Randomly Selective Frame Reversion	32
3.4 Conclusion	35
4 SYNCHRONOUS DS-MULTIBAND OFDM SYSTEM	36

TABLE OF CONTENTS
(Continued)

Chapter	Page
4.1 Signal Model	38
4.2 Receiver	43
4.3 Welsh Bound and Total Squared Correlation	45
4.4 TSC Reduction & Iterative Algorithm	48
4.5 Proposed System	48
4.6 Simulation	52
5 PERFORMANCE AGAINST INTERFERENCE	54
5.1 Types of Interference	55
5.1.1 Constant Interference	55
5.1.2 Unknown Narrowband Interference	58
5.2 Effect on user capacity of NB interference	58
6 LANCZOS ALGORITHM FOR ITERATIVE CODE GENERATION	71
6.1 Mean Square Error of the System	74
6.2 Eigendecomposition of TSC	75
6.3 Lanzos Algorithm	77
REFERENCES	90

LIST OF TABLES

Table		Page
1.1	Overview of the TI Multiband-OFDM Physical Layer Proposal Supported by the Newly Formed Multiband-OFDM Alliance	11
1.2	Overview of the Xtreme Spectrum Physical Layer Proposal	12
3.1	Scrambler Seed Selection in IEEE 802.15.3	23
3.2	Contribution of Non-Payload Data	32
4.1	Codes for Coding the User Data at Transmitter Side	52
4.2	Codes at the Receiver Side	53

LIST OF FIGURES

Figure		Page
1.1	Organization of IEEE 802.15	5
1.2	Power Spectral Density mask proposed by FCC	6
1.3	Spectrum of UWB compared with that of other wireless technologies	6
1.4	Frequency Domain and Time Domain representation of Single-band and Multiband UWB	9
3.1	Configuration of simulation of selective phase reversion	25
3.2	PSD of Multi-Band OFDM with BPSK & p=0	26
3.3	PSD of Multi-Band OFDM with BPSK & p=0.25	26
3.4	PSD of Multi-Band OFDM with BPSK & p=0.4	27
3.5	PSD of Multi-Band OFDM with QPSK & p=0	27
3.6	PSD of Multi-Band OFDM with QPSK & p=0.25	28
3.7	PSD of Multi-Band OFDM with QPSK & p=0.4	28
3.8	Configuration of scramblers	30
3.9	Comparison of initial scrambler setting: (a) original scrambler and (b) new 4-seed	31
3.10	Comparison of scrambler length: (a) LFSR-15 & 4-seed and (b) LFSR-2 & new 4-seed	31
3.11	Comparison of RFR (a) original scrambler and (b) LFSR-15 & new 4-seed & with RFR	33
3.12	Comparison of RFR (a) original scrambler and (b) LFSR-28 & new 4-seed & with RFR	34
4.1	Multiband spectrum groups of UWB	36
4.2	Grid showing the time frequency slots	39

LIST OF FIGURES
(Continued)

Figure		Page
4.3	Transmission hopping sequence in a synchronous MB-OFDM.....	40
4.4	Simplified receiver structure for synchronous DS-MB-OFDM.....	49
4.5	Receiver operation with codes assigned to transmitters.....	51
4.6	Comparison of BER for different number of users in the system and for different code lengths.....	53
5.1	Sub-carrier spread along the time-frequency grid.....	56
5.2	User capacity bound regions.....	64
5.3	Error (BER) when the interference exist in all the time frequency slots and (SIR) is -10dB.....	65
5.4	Error (BER) when the interference exist in single frequency slot and at all Times (SIR) is -10dB.....	66
6.1	Convergence comparison for reduced rank eigenspace Lanczos algorithm and MMSE replacement algorithm.....	90

CHAPTER 1

INTRODUCTION

In this chapter a short introduction to Wireless Personal Area Networks (WPANs) is provided where a brief overview of BluetoothTM is considered for extrapolating the properties of WPANs, outlining the problems classical WPAN–implementations will face in the future and finally conclude with possible features that the physical layer would need to imbibe for future WPANs. This discussion is proceeded with in the section afterwards by introducing the general ultra wide–band approach followed by brief insight into the IEEE 802.15.3a standardization process where the impulse radio based as well as FFT-IFFT based approaches are considered. A short comparison of these two techniques is also provided.

1.1 Bluetooth and Wireless Personal Area Networks

Here some properties of Bluetooth should be discussed shortly to present briefly a state of the art approach, for more details is referred to [18]. In June 2002 task group one of IEEE 802.15 published the standard adaptation of the Bluetooth PHY and MAC specification, [2]. Bluetooth has been originally developed by a consortium of the companies Ericsson, Intel, IBM, Nokia, and Toshiba with the purpose to establish a de–facto standard for example to wirelessly link cellular phones with PDAs or laptops, to link other peripheral devices, and to enable ad hoc networking. In contrast to wireless local area networks (WLANs), the focus of Bluetooth is on a smaller coverage area (10 m, communication of devices within a

personal operating space) and particularly on cheap and small devices (one–chip–solution). As establishing a connection should be possible without the direct involvement of the user and to save battery power, the devices support different sleeping modes.

A Bluetooth piconet consists of up to eight devices, one master and maximal seven slaves. As Bluetooth is designed to work without any fixed infrastructure all devices can serve either as master or slave in a piconet. Between the piconets is distinguished, by using frequency hopping. For each slot one of 79 carriers is chosen in respect to a uniquely with the piconet associated sequence. The probability of two piconets colliding is therefore 79 , if only two piconets operate next to each other. Inside the piconet the medium access is controlled by the master device with reservation and polling procedures. Let us note that here is distinguished between two kinds of medium access, in chapter 5 we come back to this. The 79 carriers are allocated in the Industrial, Scientific and Medical (ISM) band from 2.4 GHz to 2.5 GHz in one MHz distances to each other. Gaussian Frequency Shift Keying (GFSK) is used as the modulation, and the symbol rate is one Mega-baud. Data rates are supported from 57.6 kbps to 721 kbps, depending on the kind of link (synchronous/asynchronous, connection–oriented/connection-less).

From this overview over Bluetooth, following general properties of WPANs can be inferred, particularly in contrast to WLANs:

- The devices have to be particular cheap and simple, as the target applications are in low and mid price electronic devices, such as mobile phones, headsets, and PDAs, to just name the ones which are available in the presence. Further the power consumption should be particularly low, as those devices are small.
- The coverage area is small. The maximal desired range is roughly ten meters.

- There are no fixed base stations in the piconets. Every two devices can establish a piconet, even when they are in the coverage area of another piconet. The number of devices in a piconet is rather small compared to cellular networks or WLANs.
- The MAC and higher layers have to support ad hoc networking; in particular, establishing links without a setup procedure, quick joining and unjoining a piconet, and so on has to be enabled. Further an early specialization to particular applications may take place in lower layers as in Bluetooth. However, throughout the thesis we focus on the pure physical layer.

Bluetooth has after some starting problems found a big acceptance in the market and the future for WPAN approaches is promising, when one considers that they are the best choice for ubiquitous computing. As usual, applications of the future demand much higher data rates than the standard IEEE 802.15.1 supports. The taskgroup three of IEEE 802.15 addresses this by developing a new standard for WPANs with higher data rates (20 Mbps). These WPANs are supposed to operate as Bluetooth and IEEE 802.11b WLANs in the ISM–band, too. This is already one of the major problems as more and more systems operate in the 2.4 GHz ISM–band. The taskgroup two of the IEEE 802.15 working group is occupied with evaluating the mutual interference of different WPANs and WLANs operating in the ISM–band and developing coexistence mechanisms for these systems. Apart from the interference due to other wireless networks, systems have to cope in the ISM–band with the interference from complete different systems such as cordless phones (in the USA) and so on, and even microwave ovens emit a considerable amount of power in this spectrum. As has been observed in particular during the UMTS licensing procedures in Europe, available spectrum is a rare and expensive resource. As the ISM–band is with some limitations and conditions internationally free accessible, it is particular attractive. It can also be realized that in the last one or two years the usage of IEEE 802.11b for commercial and uncommercial purpose has become popular in so called “hot spots”.

Therefore, this standard is not only used in local area networks inside of commercial buildings and private homes, but also as an alternative or at least supplement to systems of the third generation. In conclusion, it is seen that the ISM will get very crowded in the future. It is difficult to construct a business case for licensing alternative spectrum for WPANs, as in particular there is no provider involved in personal area networks, who could charge a monthly fee to compensate the license expenses. Without going into any further detail into the current activities in WLAN and WPAN areas within IEEE standardization task group, Figure 1.1 gives a brief overview of all of them.

1.2 UltraWideband

As can be seen above, there exists a limitation in data rate of short range communication technology such as Bluetooth making it unviable for multimedia communications. The Shannon's channel capacity limit formula [4] shows that the channel capacity increases linearly with the bandwidth, whereas it increases logarithmically with the transmitted power. This stems the requirement to break away from the unlicensed ISM band and spread the energy over a large bandwidth thereby causing little or no interference to other technologies co-existing in the same band.

UltraWideband is a wireless technology that transmits data in a high data rate over a wide range of frequency with a very low power. UWB technology has been around since the 1960s, when the study of impulse measurement techniques revealed the potential use of pulsed based transmission in radar and communications [20]. Back at that moment, UWB was recognized by other terms, such as a carrierless, an impulse radio, and a baseband pulse. The term ultrawideband was introduced by the U.S. Department of Defense in 1989.

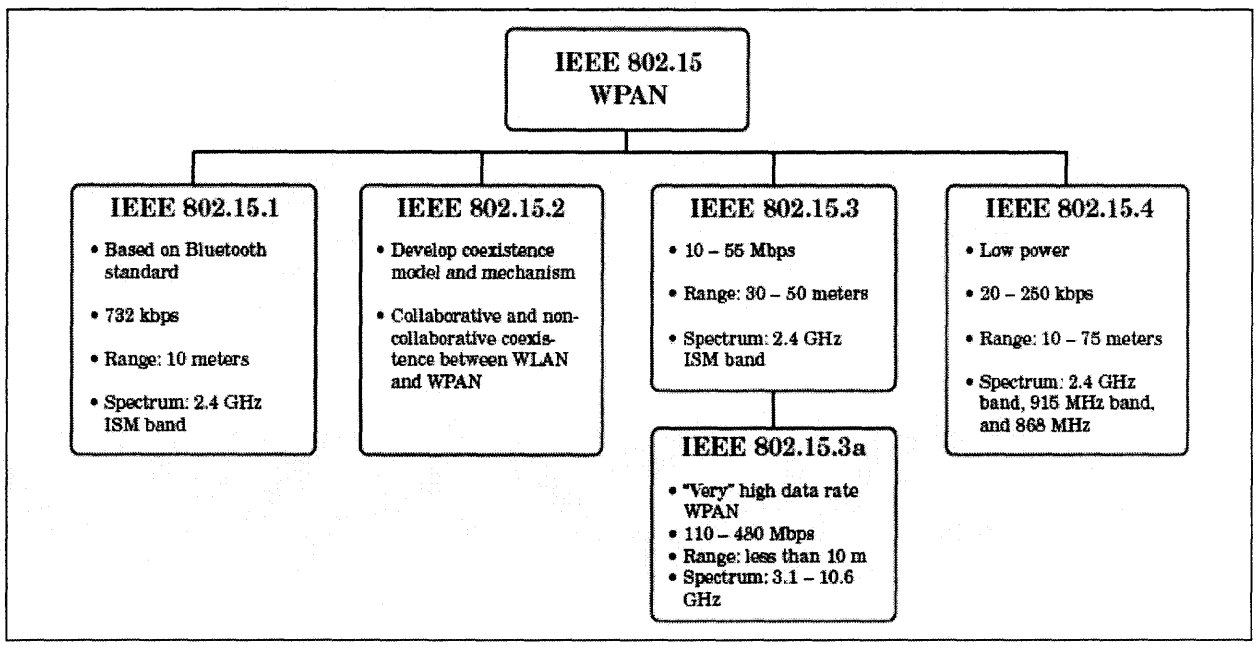

Figure 1.1 Organization of IEEE 802.15.

On February 14, 2002, the U.S. FCC issued the First Report and Order [19] that authorize the deployment of UWB technologies. Starting from that moment on, UWB systems have gained high interest among researchers and companies. The FCC defined UWB as any radio signal having a spectrum that occupy a -10 dB bandwidth of at least 500 MHz in the frequency bandwidth 3.1 - 10.6 GHz, and then the spectral mask shown in Figure 2.1 should also be fulfilled for UWB indoor communication systems. The IEEE 802.15.3a task group was entrusted with the responsibility for coming up with a standard solution allowing UWB to be commercialized under the standardization framework like the other technologies like Bluetooth, 802.11x etc.

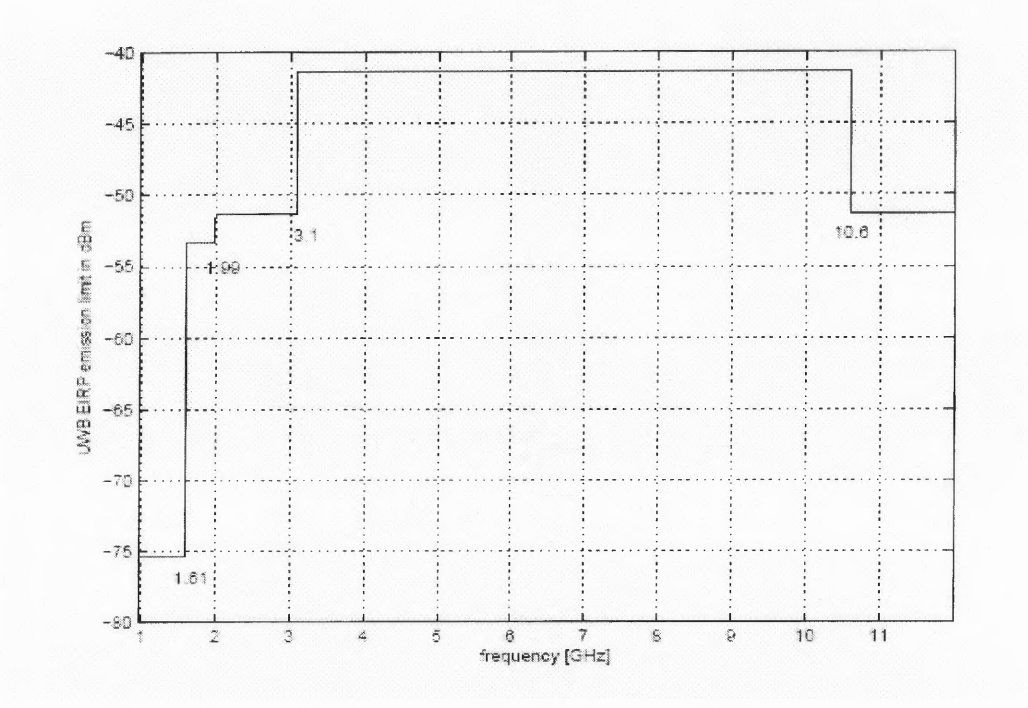

Figure 1.2 Power Spectral Density mask proposed by FCC.

The transmitted power allowed by the FCC is -41.3 dBm/MHz or basically 0.5 mW if all the 7.5 GHz bandwidth is used. This very low power causes the systems to not interfere with other existing systems over the same bandwidth, see Figure 2.2 and it can only be used in a short range communication (less than < 10 m).

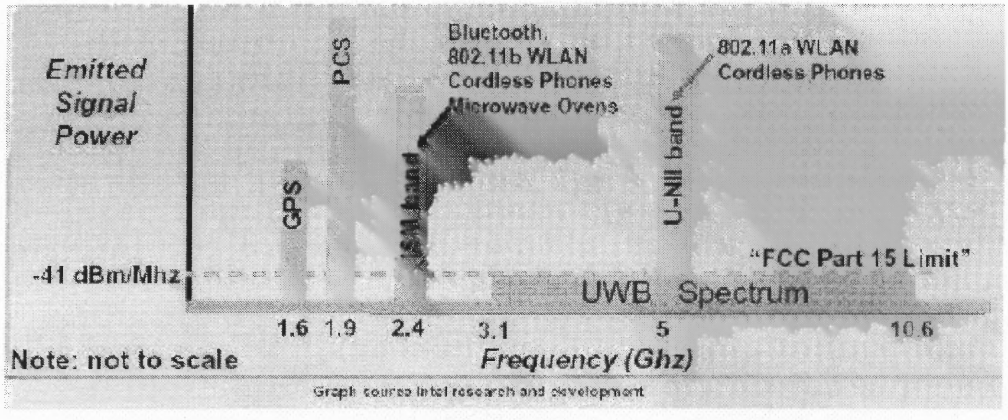

Figure 1.3 Spectrum of UWB compared with that of other wireless technologies.

The wireless indoor radio channel, which is the UWB communication systems environment, incurs a large amount of multipath fading or a large number of constructive and destructive multipath components of the transmitted pulses at the receiver. However, the UWB's large bandwidth can be used to resolve these multipath components. Having the available bandwidth of 7.5 GHz and the minimum signal bandwidth of 500 MHz, UWB systems can be divided into two groups, single band and multiband, see Figure 1.4. Both approaches offer some advantages and disadvantages, but the principles of operation are the same.

1.2.1 Single-band System

A single-band system is the traditional approach for UWB. Basically it uses a short pulse (less than 1 ns), which occupies a large bandwidth, to modulate the information. The advantage of this system is the simplicity of the transmitter design, since no carrier is needed. There are many applications based on this system, such as radar and positioning systems. A performance study of coherent Rake receivers for the single-band systems can be found in [21].

1.2.2 Multiband System

A multiband system divides the available spectrum into several smaller bands and transmits the information on each band. In this way, the spectrum flexibility increases, due to its capability to drop and select which bands to be used, and then its co-existence reliability becomes better with other systems, such as with the Wireless LAN (IEEE 802.11a) that operates in 5 GHz, see Figure 2.4. Furthermore, it is also more compliant to other

restrictive radio According to its modulation system on each band, the multiband can be divided into two systems, a pulsed multiband and a multiband based on OFDM.

The IEEE 802.15.3a task group (also called "TG3a"), established technical requirements and selection criteria for a WPAN physical layer in December 2002 and is currently debating proposals submitted by various companies, including Intel, Texas Instruments, Motorola and Xtreme Spectrum. The IEEE 802.15.3a task group set forth goals for low power consumption and low cost to ensure that the WPAN standard is amenable to implementation in CMOS technology. These requirements will ensure that the high data rate physical layer drafted by 802.15.3a can be easily integrated into WPAN devices which have MAC and network layers already implemented in CMOS technology [22].

The UWB Multiband-Coalition (www.uwbmultiband.org) which was led initially by Intel included several other major companies that supported a multiband approach which employs pulsed modulation. On July 14, 2003, industry titans Intel and Texas Instruments merged their proposals to form a united approach that employs multiple bands and uses OFDM modulation. The newly formed Multiband-OFDM Coalition (www.multibandofdm.org), whose membership includes TI and the UWB Multiband-Coalition, endorses a proposal which is essentially the same as the original TI proposal, with an optional operating mode which uses seven bands (as opposed to three). Currently TG3a is has two primary contenders: (1) The Texas Instruments OFDM-based multiband approach which uses 528 MHz channels (three mandatory lower band channels and four optional upper band channels) supported by the Multiband-OFDM Coalition, and (2) the

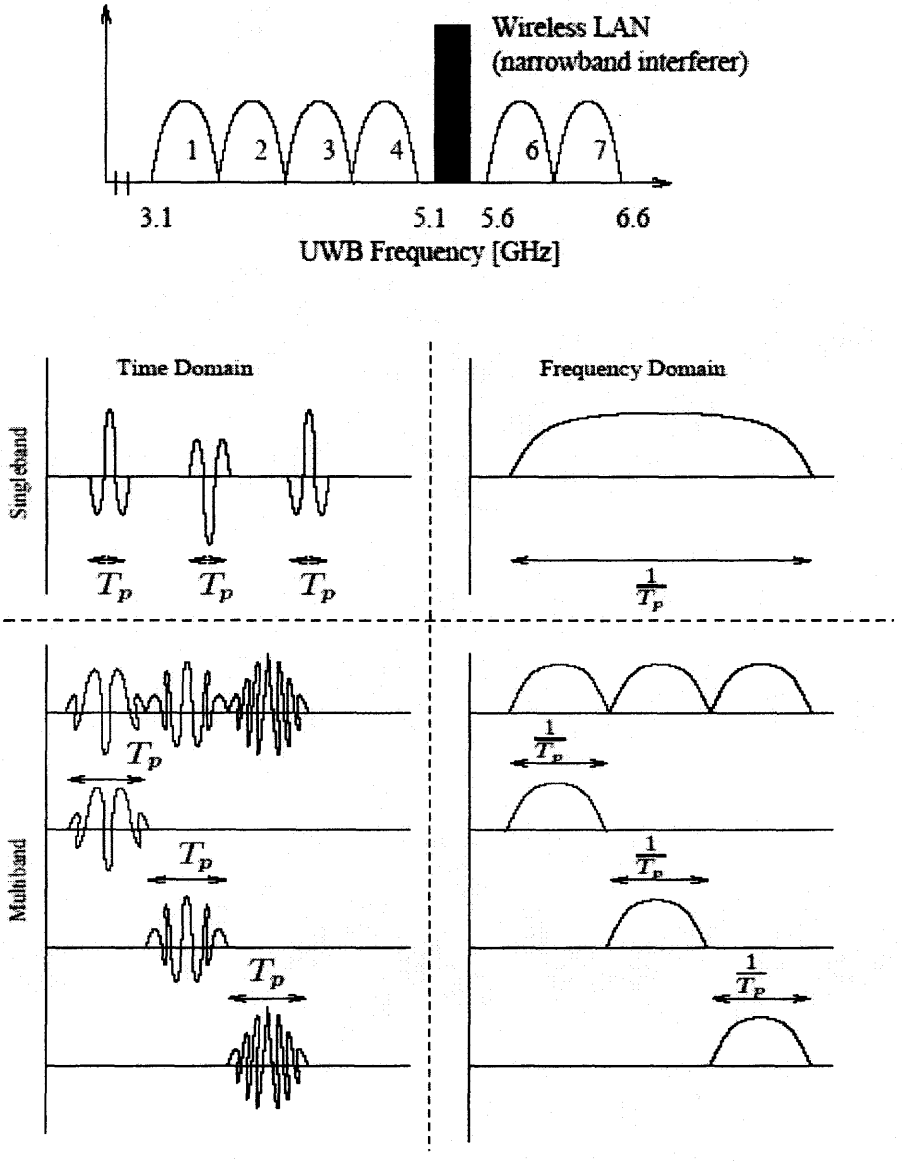

Figure 1.4 Topmost figure shows coexistence of Multiband UWB and narrowband interference. The following figure gives comparison of single band and Multiband UWB both in time domain and frequency domain.

Xtreme Spectrum-Motorola dual-band Impulse Radio spread spectrum approach, where there is a high band (above the 5.2 - 5.8 GHz unlicensed band) and a low band (from 3.1 GHz to just below the 5.2 - 5.8 GHz unlicensed band), and which exploits all of the UWB

spectrum allocation. Table 1.1 and 1.2 give an overview of the proposals from each of the two contenders.

As shown in Table 1.1, Texas Instruments prefers a channelized UWB system. There are three Group A bands which are used for standard operation. The four Group C bands are allocated for optional use in areas where simultaneous operating piconets are in close proximity (this is only used at close proximity since propagation loss severely limits signals at these higher frequencies). Group B and D bands are reserved for future expansion. Each band uses frequency hopping orthogonal frequency division multiplexing (TFIOFDM), which allows for each UWB band to be divided into a set of orthogonal narrowband channels (with much larger symbol period duration). Because of the increased length of the OFDM symbol period, this modulation method can successfully reduce the effects of ISI. However, this robust multipath tolerance comes at the price of increased transceiver complexity, the need to combat inter-carrier interference (ICI), and tighter linear constraint on amplifying circuit elements. The University of Minnesota also proposed a similar OFDM approach [18].

Table 1.1 Overview of the TI Multiband-OFDM Physical Layer Proposal Supported by the Newly Formed Multiband-OFDM Alliance

Spectrum Allocation	
No. of bands	3 (1st generation bands), 10 optional bands
Bandwidths	528 MHz
Frequency ranges	Group A: 3.168-4.752 GHz Group B: 4.752-6.072 GHz Group C: 6.072-8.184 GHz Group D: 8.184-10.296 GHz
Modulation scheme	TFI-OFDM (with 128-point FFT), QPSK
Coexistence method	Null band for WLAN (~5 GHz)
Multiple access method	Time-frequency interleaving
No. of simultaneous piconets	4
Error correction codes	Convolutional code
Code rates	11/32 @ 110 Mbps, 5/8 @ 200 Mbps 3/4 @ 480 Mbps
Link margin	5.3 dB @ 10 m @ 110 Mbps 10.0 dB @ 4 m @ 200 Mbps 11.5 dB @ 2 m @ 480 Mbps
Symbol period	312.5 ns OFDM symbol
Multipath mitigation method	1-tap (robust to 60.6 ns delay spread)

The Xtreme Spectrum-Motorola proposal uses a dual band approach, as shown in Table 1.2, which employs short duration pulses to transmit over each band, having bandwidth in excess of 1 GHz (this is often referred to as impulse radio). Xtreme Spectrum's design benefits from a coding-gain achieved through the use of direct sequence spread spectrum (DS-SS) with 24 chips/symbol, and exploits the Hartley Shannon principals to a greater degree than the Multiband-OFDM approach, has greater precision for position location, and realizes better spectrum efficiency.

Table 1.2 Overview of the Xtreme Spectrum Physical Layer Proposal

Spectrum Allocation	
No. of bands	2
Bandwidths	1.368 GHz, 2.736 GHz
Frequency ranges	3.2 – 5.15 GHz 5.825 – 10.6 GHz
Modulation scheme	BPSK, QPSK, DS-SS
Coexistence method	Null band for WLAN (~5 GHz)
Multiple access method	Ternary CDMA
No. of simultaneous piconets	8
Error correction codes	Convolutional code, Reed-Solomon code
Code rates	1/2 @ 110 Mbps RS(255,223) @ 200 Mbps RS(255,223) @ 480 Mbps
Link margin	6.7 dB @ 10 m @ 114 Mbps 11.9 dB @ 4 m @ 200 Mbps 1.7 dB @ 2 m @ 600 Mbps
Chip time	731 ps (Low band), 365.5 ps (High band)
Multipath mitigation method	Decision feedback equalizer and RAKE

However, it has less flexibility with regard to foreign spectral regulation and may be too broadband if foreign governments choose to limit their UWB spectral allocations to smaller ranges than authorized by the FCC. Sony [23] and Parthus Ceva [24] also have offered similar proposals which employ DS-SS over very wide bandwidths.

Having introduced the two possible Multiband transmission schemes, the thesis shall consider Multiband-OFDM scheme in the following chapters. The thesis deals primarily with two issues, of power spectral density of MB-OFDM and user capacity of MB-OFDM under current scheme chalked out by MBOA. Chapter 3 takes a look at the former and shows that the discrete line spectra are an issue in MB-OFDM that needs to be addressed. It also discusses mechanism of increased length LFSR, a new set of seeds and Random Phase

Reversion for removal of line spectra leading to baseband whitening. Chapter 4 addresses the issue of user capacity of the current proposed MB-OFDM system whereby iteratively generated codes based on MMSE algorithm are used to overcome the limitation and allow more users into the system. A whole new structure for meeting the future wireless needs is discussed wherein communication is overlooked by a central controller. The system of coded communication is further analyzed for performance against interference in Chapter 5. Interestingly, the codes are shown to somewhat adapt to the interfering environment implying possible operation of the band for a given QoS with interference present. Expressions for user capacity bounds under the interference are also derived. In Chapter 6, design simplifications through reduced computations for generating the codes are considered. It introduces Lanczos algorithm for two different approaches of computing the codes. The need for simplified design stems largely from the need for having large number of MMSE units for code generation. Thus, Chapters 4-6 take a complete look at the problem at hand from providing a theoretical solution and alongside provide algorithms for simplifying the system from design point of view.

CHAPTER 2

POWER SPECTRAL DENSITY OF CYCLOSTATIONARY PROCESSES

In this chapter power spectral density (PSD) [26] of stochastic processes involving signals carrying digital information that are periodic in nature are considered. After providing the necessary background, the resulting expressions for power spectral density are used in Chapter 3 for evaluating and analyzing PSD of Multiband-OFDM signal.

2.1 Cyclostationary Process

In dealing with signals that carry digital information we encounter stochastic processes that have statistical averages that are periodic. To be specific, let us consider a stochastic process of the following form

$$X(t) = \sum_{n=-\infty}^{\infty} I_n g(t - nT) \tag{2.1}$$

where $\{I_n\}$ is a discrete time sequence of random variables with mean $m_I = E[I_n]$ for all n and autocorrelation sequence $\phi_{II}(k) = E[I_n^* I_{n+k}]$. The signal $g(t)$ is deterministic. $X(t)$ is a generalized stochastic process representing a linear modulated signal. The $\{I_n\}$ represents the digital information sequence that is transmitted over the communication channel and 1/T represents the rate of transmission of the information symbols.

The mean and autocorrelation of the generalized stochastic process $X(t)$ can be determined as shown below

$$E[X(t)] = E\left[\sum_{n=-\infty}^{\infty} I_n g(t-nT)\right]$$

$$= m_I \sum_{n=-\infty}^{\infty} g(t-nT) \tag{2.2}$$

One can easily observe that the mean is time-varying. Infact, it is periodic with period T. The autocorrelation function of $X(t)$ is

$$\phi_{xx}(t+\tau,t) = E[X(t+\tau)X^*(t)]$$

$$= \sum_{n=-\infty}^{\infty}\sum_{m=-\infty}^{\infty} E[I_n^* I_m] g^*(t-nT)g(t+\tau-mT)$$

$$= \sum_{n=-\infty}^{\infty}\sum_{m=-\infty}^{\infty} \phi_{II}(m-n) g^*(t-nT)g(t+\tau-mT) \tag{2.3}$$

Again, observing the periodicity of autocorrelation function which is illustrated below.

$$\phi_{xx}(t+\tau+kT,t+kT) = \phi_{xx}(t+\tau,t) \tag{2.4}$$

Such a stochastic process is called cyclostationary or periodically stationary. Since the autocorrelation function depends on both the variables t and τ, its frequency domain representation requires 2D Fourier transform.

However, it is more desirable to characterize such signals by their power density spectrum and so an alternative approach of computing time-average autocorrelation function over a single period thereby removing the function's dependency on time variable, is employed.

$$\bar{\phi}_{xx}(\tau) = \frac{1}{T}\int_{-T/2}^{T/2} \phi_{xx}(t+\tau, t)dt \tag{2.5}$$

Now the Fourier transform of the averaged autocorrelation functions yields average power spectral density of cyclostationary process.

$$\Phi_{xx}(f) = \int_{-\infty}^{\infty} \bar{\phi}_{xx}(\tau)e^{-j2\pi ft}dt \tag{2.6}$$

2.2 PSD of Linearly Modulated Signal

In order to understand the effect of modulation and the sequence of information symbols transmitted, consider the results developed in previous section and evaluate expression (2.6). As established before, the power spectral density requires averaging of time varying autocorrelation function followed by Fourier transform of the averaged auto-correlation function.

Let us first consider (2.4)

$$\begin{aligned}\phi_{xx}(t+\tau, t) &= \sum_{n=-\infty}^{\infty}\sum_{m=-\infty}^{\infty} \phi_{II}(m-n)g^*(t-nT)g(t+\tau-mT) \\ &= \sum_{m=-\infty}^{\infty} \phi_{II}(m)\sum_{n=-\infty}^{\infty} g^*(t-nT)g(t+\tau-nT-mT)\end{aligned} \tag{2.7}$$

Averaging (2.7) over one complete time period gives

$$\begin{aligned}\bar{\phi}_{xx}(\tau) &= \frac{1}{T}\int_{-T/2}^{T/2} \phi_{xx}(t+\tau, t)dt \\ &= \sum_{m=-\infty}^{\infty} \phi_{II}(m)\sum_{n=-\infty}^{\infty} \frac{1}{T}\int_{-T/2}^{T/2} g^*(t-nT)g(t+\tau-nT-mT)dt \\ &= \sum_{m=-\infty}^{\infty} \phi_{II}(m)\sum_{n=-\infty}^{\infty} \frac{1}{T}\int_{-T/2-nT}^{T/2-nT} g^*(t)g(t+\tau-mT)dt\end{aligned} \tag{2.8}$$

The integral in the above expression can be interpreted as time-autocorrelation function of g(t) and define it as

$$\phi_{gg}(\tau) = \int_{-\infty}^{\infty} g^*(t)g(t+\tau)dt \tag{2.9}$$

Consequently (2.9) can be expressed as

$$\bar{\phi}_{xx}(\tau) = \frac{1}{T}\sum_{m=-\infty}^{\infty} \phi_{II}(m)\phi_{gg}(\tau - mT) \tag{2.10}$$

The Fourier transform of above yields the power spectral density of the [] which is given as

$$\Phi_{xx}(f) = \frac{1}{T}|G(f)|^2 \Phi_{II}(f) \tag{2.11}$$

where $G(f)$ is the Fourier transform of the signal $g(t)$, and $\Phi_{II}(f)$ denotes the power spectral density of information sequence, defined as

$$\Phi_{II}(f) = \sum_{m=-\infty}^{\infty} \phi_{II}(m)e^{-j2\pi fmT} \tag{2.12}$$

The result illustrates the dependence of the power spectral density of $X(t)$ on the spectral characteristics of the pulse $g(t)$ and the information sequence $\{I_n\}$. That is, the spectral characteristics of $X(t)$ can be controlled by the design of the pulse shape $g(t)$ and by design of the correlation characteristics of the information sequence.

In order to comprehend the subtle effect that the correlation characteristics bear on the overall spectral density of the linearly modulated signal, let us consider the case in which the information symbols in the sequence are real and mutually uncorrelated. In this case, autocorrelation function $\phi_{II}(m)$ can be expressed as

$$\phi_{II}(m) = \begin{cases} \sigma_I^2 + m_I^2 & (m = 0) \\ m_I^2 & (m \neq 0) \end{cases} \tag{2.13}$$

where σ_I^2 denotes variance of an information symbol. When (2.13) is substituted for $\phi_{II}(m)$ in (2.12), we obtain

$$\Phi_{II}(f) = \sigma_I^2 + m_I^2 \sum_{m=-\infty}^{\infty} e^{-j2\pi fmT} \tag{2.14}$$

The summation in (2.14) is periodic with period 1/T. It may be viewed as the exponential Fourier series of a periodic train of impulses with each impulse having an area 1/T. Therefore (2.14) can also be expressed in the form

$$\Phi_{II}(f) = \sigma_I^2 + \frac{m_I^2}{T} \sum_{m=-\infty}^{\infty} \delta\left(f - \frac{m}{T}\right) \tag{2.15}$$

Substitution of (2.15) into (2.11) yields the desired result for the power density spectrum of $X(t)$ when the sequence of information symbols is uncorrelated. That is,

$$\Phi_{xx}(f) = \frac{\sigma_I^2}{T}|G(f)|^2 + \frac{m_I^2}{T^2} \sum_{m=-\infty}^{\infty} \left|G\left(\frac{m}{T}\right)\right|^2 \delta\left(f - \frac{m}{T}\right) \tag{2.16}$$

Clearly evident from above is that the spectrum density has two distinct components. One is the continuous part which depends on the Fourier transform of the waveform signal $g(t)$ and second is the discrete part which consists of terms spaced 1/T apart in frequency. Each spectral line has power proportionate to $|G(f)|^2$ evaluate at $f = m/T$. The discrete lines in the spectrum density vanish when $m_I = 0$ i.e. when information symbols have zero mean. This condition is usually desirable and is satisfied when information symbols are equally likely and symmetrically positioned in the complex plane.

CHAPTER 3

BASE-BAND DATA WHITENING OF MULTI-BAND OFDM UWB SIGNALS

With declassification of the UWB by the FCC allowing it to be used for commercial purposes, there has been extensive effort put into research & development and standardization [3]. UWB is now under consideration as an alternative physical layer technology for wireless PAN.

The key motivation for the FCC's new decision is that no new spectrum would be required because UWB signals can CO-exist with other applications in the same spectrum with negligible mutual interference. Therefore the FCC has specified emission limits for the UWB applications. A basic requirement by the FCC is that UWB systems do not generate interference to other narrowband communication systems.

Evaluation of the Power Spectral Density (PSD) for ideal synchronous data pulse streams based upon stochastic theory is well documented in the literature [3, 4]. According to the above research, power spectra of UWB signals consist of continuous and discrete components. The discrete component presents greater interference to narrowband communication systems than the continuous component. Thus a basic objective in the design of UWB systems is to reduce the discrete component of the UWB power spectrum. Schemes to suppress discrete component were proposed in [5, 6].

With the emergence of a new modulation technology called Multi-Band OFDM (MB-OFDM), working frequency band of UWB systems is divided into sub-bands and in each sub-band OFDM modulation is used. Because it is so new that little research was

reported in the literature on whether lines in spectrum is an issue for MB-OFDM and how to reduce the PSD of signals in MB-OFDM UWB systems.

This chapter demonstrates by analysis and simulation that line spectra is still an issue for MB-OFDM UWB systems. A mechanism is proposed to remove lines in the PSD, therefore reduce the PSD in each sub-band.

3.1 Current Implementation in Wireless Systems

In this section, PSD of a MB-OFDM UWB sequence proposed to IEEE 802.15.3a will be investigated and study the scrambler in the MB-OFDM UWB proposal to IEEE 802.15.3a.

3.1.1 PSD of MB-OFDM UWB

In the MB-OFDM UWB Communication Systems, a digitally controlled signal is used that produces random transmissions at multiples of the basic clock period *Ts*. This signaling technique can be modeled as

$$s(t) = \sum_{n=-\infty}^{\infty} \mathrm{Re}\left\{ \sum_{k=-\frac{N_s}{2}}^{\frac{N_s}{2}-1} d_{n,k+\frac{N_s}{2}} \exp\left(j2\pi (f_n - \frac{k+0.5}{T})(t - nT_s) \right) \right\} \qquad (3.1)$$

$$f_n \in \{f_m : m = 1, \ldots, M\}, \qquad nT_s \le t \le nT_s + T$$

where $\{ d_{n,k+N_s/2} \}$ is an unbalanced binary independent identically distributed (i.i.d.) random sequence, and $\{f_m\}$ is the center frequency of each sub-band.

If M bands are used and OFDM symbols are transmitted on sub-band in turns, waveform of carrier k in band m can be expressed as

$$s_{m,k}(t) = \sum_{n=-\infty}^{\infty} \mathrm{Re}\left\{ d_{n,k+\frac{N_s}{2}} \exp\left(j2\pi(f_m - \frac{k+0.5}{T})(t-(nM+m)T_s) \right) \right\} \tag{3.2}$$
$$1 \le m \le M, \qquad (nM+m)T_s \le t \le (nM+m)T_s + T$$

If BPSK modulation is used on each carrier, waveform of carrier k on sub-band m can be expressed as

$$s_{m,k}(t) = A_1 \sum_{n=-\infty}^{\infty} a_{n,m,k} w_{m,k}\left(t-(nM+m)T_s\right) \tag{3.3}$$

where A_1 is the scale coefficient and

$$w_{m,k}(t) = \cos\left(2\pi(f_m - \frac{k+0.5}{T})t \right) \tag{3.4}$$

and

$$\Pr\{a_{n,m,k}\} = \begin{cases} p, & a_{n,m,k} = 1 \\ 1-p, & a_{n,m,k} = -1 \end{cases} \tag{3.5}$$

For QPSK modulations, waveform of carrier k on band m can be expressed as

$$s_{m,k}(t) = A_2 \sum_{n=-\infty}^{\infty} a_{n,m,k} w_{m,k}\left(t-(nM+m)T_s\right) \tag{3.6}$$

where A_2 is the scale coefficient and

$$w_{m,k}(t) \in \left\{ \cos\left(2\pi(f_m - \frac{k+0.5}{T})t \right) + \Phi_l : l = 1,2, \quad |\Phi_1 - \Phi_2| = \pi/4 \right\} \tag{3.7}$$

and

$$\Pr\{a_{n,m,k}\} = \begin{cases} p, & a_{n,m,k} = 1 \\ 1-p, & a_{n,m,k} = -1 \end{cases} \tag{3.8}$$

Similar to operations shown in [3][4][6][7], and also observed in previous chapter, the PSD of the signals consist of continuous component and discrete component and both components can be expressed as

$$\begin{aligned} S^c_{m,k}(f) &= \frac{1-(2p-1)^2}{MTs}\left|W_{m,k}(f)\right|^2 \\ S^d_{m,k}(f) &= \frac{(2p-1)^2}{(MTs)^2}\sum_{l=-\infty}^{\infty}\left|W_{m,k}(\frac{l}{MTs})\right|^2 \delta_D(f-\frac{l}{MTs}) \end{aligned} \tag{3.9}$$

The total PSD is the superimposition of the two spectra of waveforms described in equation (3.9).Equation (3.9) indicates that the PSD is determined by four factors, i.e.,

- $W_{m,k}(f)$ – pulse shape and transmission power of carrier k in sub-band m
- Ts – clock period or pulse rate
- p – distribution of a_n
- M – total number of sub-bands

Similar to the analysis in [6], when

$$p = 0.5 \tag{3.10}$$

lines in each sub-band can be removed, therefore the PSD on each sub-band get minimized. The new PSD can be expressed as

$$\begin{aligned} S^c_{m,k}(f) &= \frac{1}{MTs}\left|W_{m,k}(f)\right|^2 \\ S^d_{m,k}(f) &= 0, \qquad -\frac{N_s}{2} \le k \le \frac{N_s}{2}-1 \qquad and \qquad 1 \le m \le M \end{aligned} \tag{3.11}$$

3.1.2 Current Scrambler in MB-OFDM Proposal to IEEE 802.15.3a

Major system proposals to IEEE 802.15.3a employ IEEE 802.15.3 MAC, a TDMA system, and Scrambler, a 15-bit Linear Feedback Shift Register (LFSR) to generate pseudo random binary sequence (PRBS).

In IEEE 802.15.3, the scrambler is applied to payload data and some upper layer data. At the beginning of each frame, the scrambler is loaded with predefined values, which will be called as initial setting for the rest of this paper. Four seeds are defined for selection as initial setting, shown in Table 3.1.

Table 3.1 Scrambler Seed Selection in IEEE 802.15.3

Seed identifier (b_1, b_0)	Seed value (x_{14} ... x_0)
0,0	0011 1111 1111 111
0,1	0111 1111 1111 111
1,0	1011 1111 1111 111
1,1	1111 1111 1111 111

3.2 Proposed Mechanism

In this section, mechanism of phase reversion to reduce PSD of MB-OFDM UWB signals and new scrambler design for MB-OFDM UWB systems to the IEEE 802.15.3a.is proposed. Simulation analysis is provided for above design.

3.2.1 Phase Reversion to Minimize PSD of MB-OFDM UWB Signals

In this sub-section, a mechanism of phase reversion to reduce PSD of MB-OFDM UWB signals is proposed followed by simulation analysis.

3.2.1.1 Phase Reversion to Minimize PSD in Sub-bands. Based on the preceding analysis of the PSD of multi-band UWB signals, following mechanism of selective phase reversion to eliminate line frequencies is proposed:

1. Generating a random sequence $\{b_{n,m,k}\}$ with the evenly distributed function of

$$\Pr\{b_{n,m,k}\} = \begin{cases} 0.5, & b_{n,m,k} = 1 \\ 0.5, & b_{n,m,k} = -1 \end{cases} \tag{3.12}$$

2. Performing an exclusive OR (*XOR*) operation on sequences $\{a_{n,m,k}\}$ and $\{b_{n,m,k}\}$ to produce a new sequence $\{c_{n,m,k}\}$. The $\{c_{n,m,k}\}$ is used as the new data for transmission.

$$c_{n,m,k} = a_{n,m,k} \wedge b_{n,m,k} \tag{3.13}$$

Similar to [6], it can be proved that performing the above operation will remove lines in PSD of UWB signals in each sub-band. This is equivalent to minimize PSD in each sub-band.

3.2.1.2 Simulation Analysis. Simulations were performed to show that line spectra is still an issue for MB-OFDM systems. The simulation also showed that applying the operation proposed in equation (3.12) and (13) will suppress line spectra and reduce the PSD of MB-OFDM signals.

`The configuration of the simulations is shown in Figure 3.1. The simulations use Periodogram PSD estimators to calculate the PSD of different UWB signals. Only one sub-band is used in the simulation. In the configuration of the simulation, an OFDM symbol consists of 16 carriers, which is represented by 160 samples including Cyclic Prefix followed by 96 samples of zero padding as guard time. One frame contains 256 symbols. FFT is performed on frames, i.e., 64K-point FFT on 64K samples to evaluate the PSD. Because a single estimate usually generates a large bias in estimation and the

FCC regulation sets a limit on average PSD, 100 runs are used to smooth the final PSD estimate.

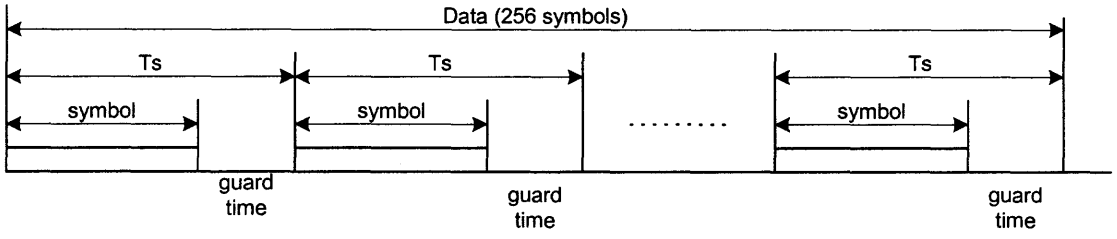

Figure 3.1 Configuration of simulation of selective phase reversion.

Simulation results are shown in Figure 3.2 to 3.7. In these figures, panel (a) is the PSD of original data $\{a_{n,m,k}\}$ and panel (b) is the PSD of resulting data $\{c_{n,m,k}\}$ after operations described in equation (3.12) and (3.13).

Figure 3.2 to 3.4 depict simulation results with BPSK modulation. And Figure3.5 to 3.7 depict simulation results with QPSK modulation.

The results indicate that, with this method:

- Line spectra will appear if original data $\{a_{n,m,k}\}$ is not evenly distributed no matter BPSK or QPSK is used;

- Selective phase reversion performed on original data can remove spectra lines. Because of above reason, peak value of PSD is reduced accordingly from about –4.8 dB, -14 dB and –23 dB to about -31 dB for BPSK modulation shown in Figure 3.2 to 3.4, and from about –7.8 dB, -17 dB and –26 dB to about –34 dB for QPSK modulation shown in Figure 3.5 to 3.7;

- No matter what is the PSD of original data, the PSD of processed data is almost the same, i.e., -31 dB for BPSK modulation and –34 for QPSK modulation.

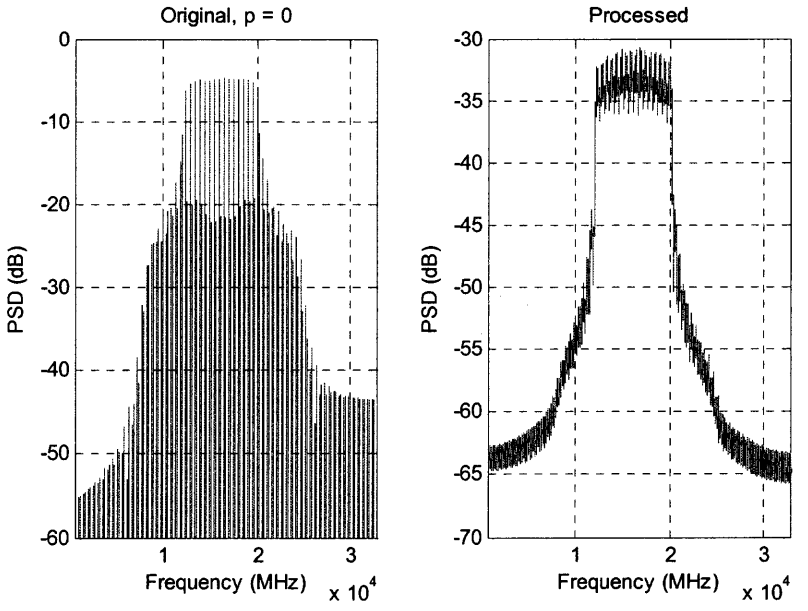

Figure 3.2 PSD of Multi-Band OFDM with BPSK & p=0.

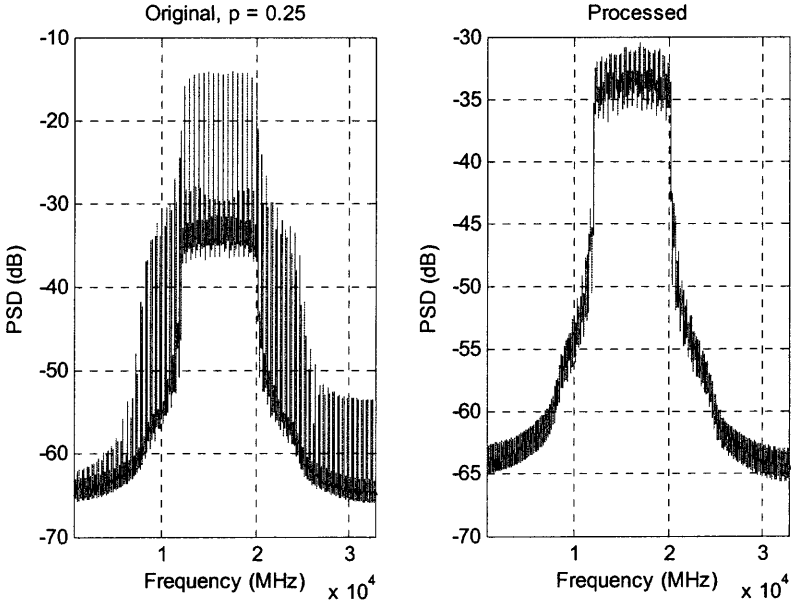

Figure 3.3 PSD of Multi-Band OFDM with BPSK & p=0 .25.

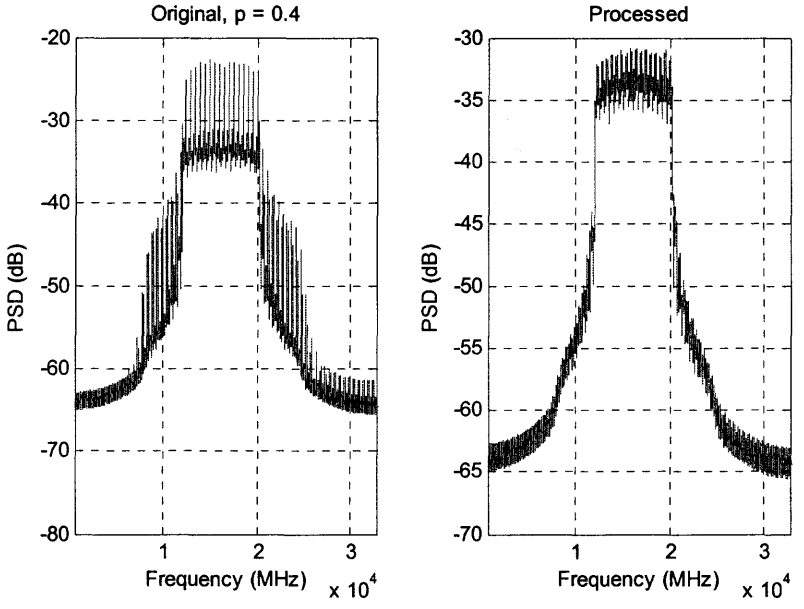

Figure 3.4 PSD of Multi-Band OFDM with BPSK & p=0.4.

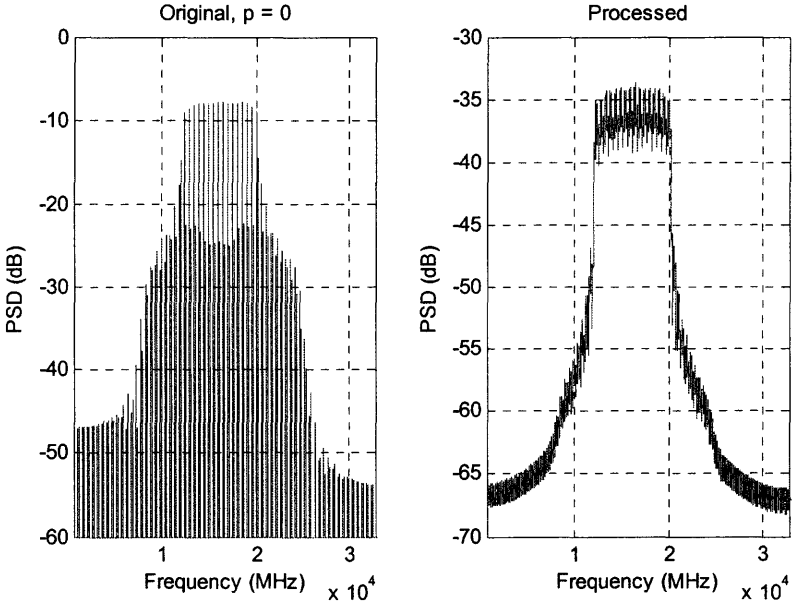

Figure 3.5 PSD of Multi-Band OFDM with QPSK & p=0

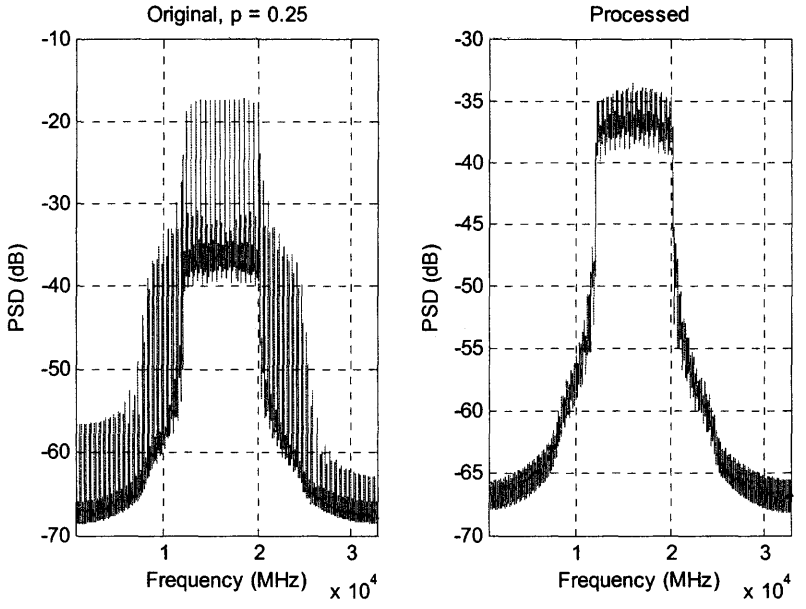

Figure 3.6 PSD of Multi-Band with QPSK & p=0.25.

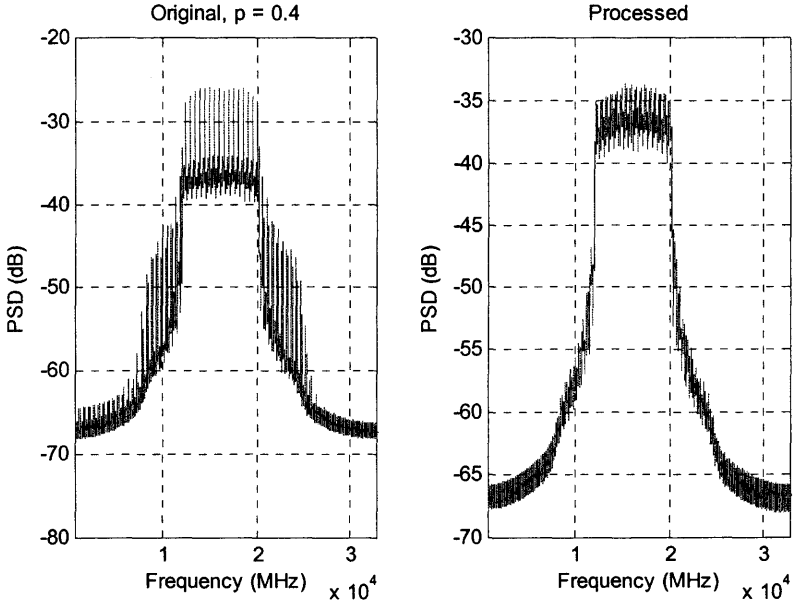

Figure 3.7 PSD of Multi-Band OFDM with QPSK& p=0.4.

3.3 Scrambler Design for MB-OFDM UWB System to IEEE 802.15.3a

In this sub-section, a new scrambler design for MB-OFDM UWB system to IEEE 802.15.3a is proposed. Simulation analysis is provided.

3.3.1 New Four Seeds for Scramblers

It has been shown that the scramblers using original four seeds generate strong spectral lines [8]. Although it is for single band impulse based UWB systems, it is shown later that for MB-OFDM UWB systems, the scramblers generate strong spectral lines too. This observation suggested that other sets of seeds that are independent from each other would give a better randomness in scrambler setting. As such, new four seeds to increase randomness of initial setting of scrambler, thus increasing randomness in the Y direction described in [8] is proposed.

Simulation on a different initial setting of scrambler is conducted. Configuration of the simulation is given in Figure 3.8, in which frame rate is 128 frames/second and one frame contains 256 symbols. Each symbol has 16 carriers that come from the first 16 carriers in the 128 carriers that are used in original MB-OFDM UWB systems. Payload data are all "1"s to the scrambler and no non-payload data. The simulation results are shown in Figure 3.9 in which (a) uses original scrambler, or LFSR-15 with original four seeds, which is given in Table 3.1, and (b) LFSR-15 with new four seeds that are generated by MATLAB rand() function. The result showed that the scrambler with new four seeds reduces the PSD by about 16dB.

3.3.2 LFSR-28 for Scramblers

In Figure 3.9(b), strong spectra lines still exist. These lines are associated with the short length of polynomial generator for PRBS. To further reduce these lines, a longer polynomial generator, LFSR-28, is proposed [8]. Simulation is performed and result is given in Figure 3.10, in which (a) uses original scrambler, or LFSR-15 with original four seeds and (b) LFSR-28 with new four seeds. Results in Figure 3.9(b) and Figure 3.10(b) showed that the using LFSR-28 reduces the PSD by additional about 3dB.

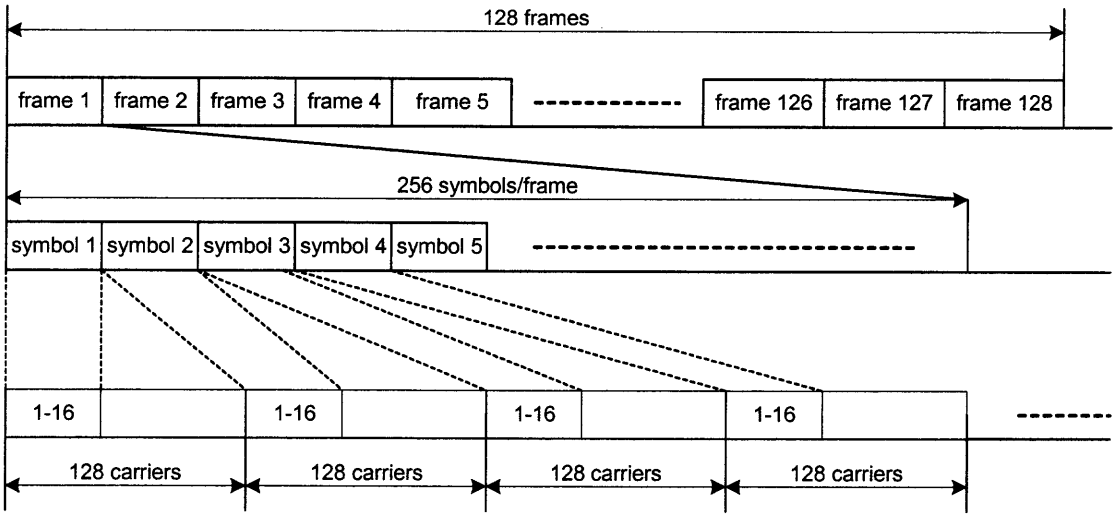

Figure 3.8 Configuration of scramblers.

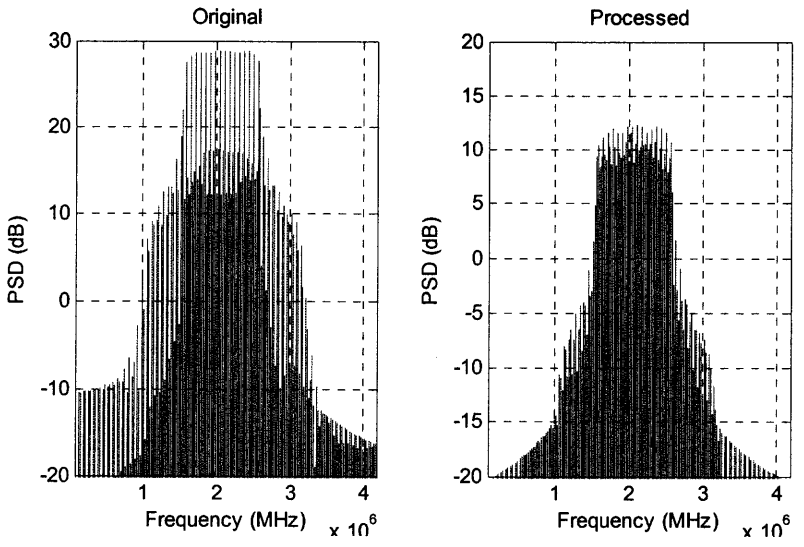

Figure 3.9 Comparison of initial scrambler setting: (a) original scrambler and (b) new 4-seed.

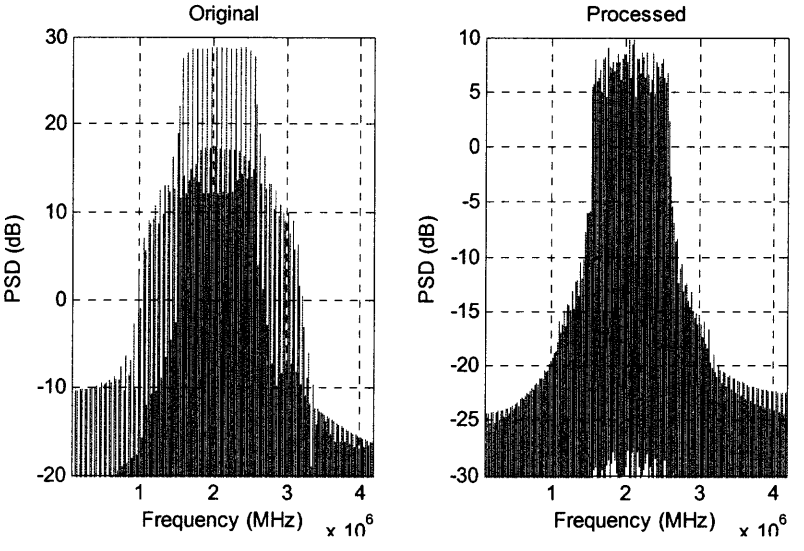

Figure 3.10 Comparison of scrambler length: (a) LFSR-15 & 4-seed and (b) LFSR-2 & new 4-seed.

3.3.3 Randomly Selective Frame Reversion

Since IEEE 802.15.3a utilizes IEEE 802.15.3 MAC, the maximal frame length would be 2KByte. Assume a video stream needs 16Mbps bandwidth, the minimal PRF of frames would be

$$\begin{aligned} 16M/(2K*8) &= 1K \\ T_f &= 10^{-3} \end{aligned} \tag{3.14}$$

Because $T_f<<1$, non-payload data will generate strong lines. Table 1 lists some values the non-payload data contributes to PSD with assumption of $T_f=10^{-3}$, where p_{st} is the percentage of non-payload data in the stream. This table indicates that although non-payload data constitutes small portion in frames, their contribution to PSD cannot be neglect due to high PRF of the frames. If a smaller frame length is used in harsh environment to reduce frame error rate, the same percentage of non-payload data will generate stronger spectral lines and more PSD than those listed in Table 2.

Table 3.2 Some values for equation (3.4)

p_{sl}	**ΔPSD (dB)**
0.1%	3.01
0.5%	7.78
1%	10.41
5%	17.07
10%	20.04

To reduce the PSD generated by non-payload data, a scheme of random frame reversion (RFR) is proposed. For easy understanding, framed data stream can be expressed as

$$s(t) = \sum_{l=-\infty}^{\infty} \sum_{k=1}^{K} a_{l,k} w(t - lT_f - kT_p) \tag{3.15}$$

where l and k are index of frames and pulses in frames.

The RFR is able to reduce spectra lines generated by non-payload data, which is not scrambled. It works as follows [6]:

- A random sequence $\{b_n\}$ is generated with evenly distributed function of

$$\Pr\{b_n\} = \begin{cases} 0.5, & b_n = 1 \\ 0.5, & b_n = -1 \end{cases} \tag{3.16}$$

- The following operation is applied to data and sequence to produce a new sequence

$$c_{l,k} = \begin{cases} a_{l,k}, & b_l = 1 \\ -a_{l,k}, & b_l = -1 \end{cases} \tag{3.17}$$

- $\{c_{l,k}\}$ is transmitted as new data

The RFR can also further reduce the PSD of the payload data.

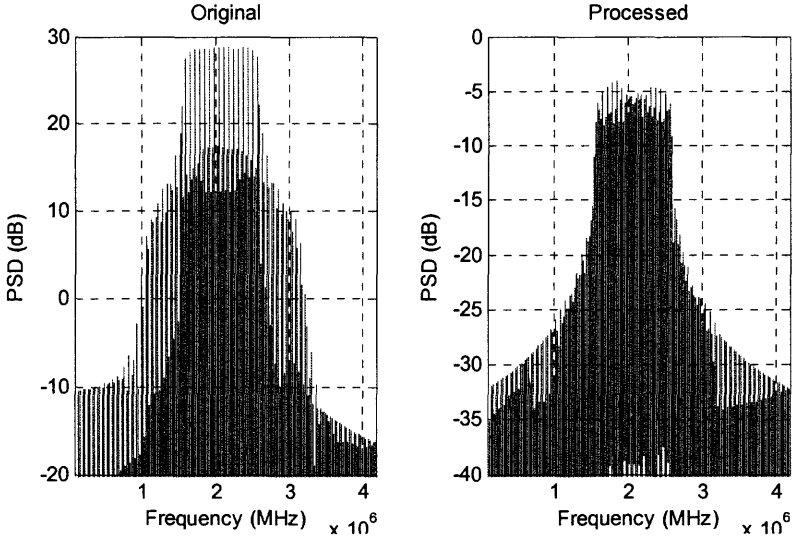

Figure 3.11 Comparison of RFR (a) original scrambler and (b) LFSR-15 & new 4-seed & with RFR.

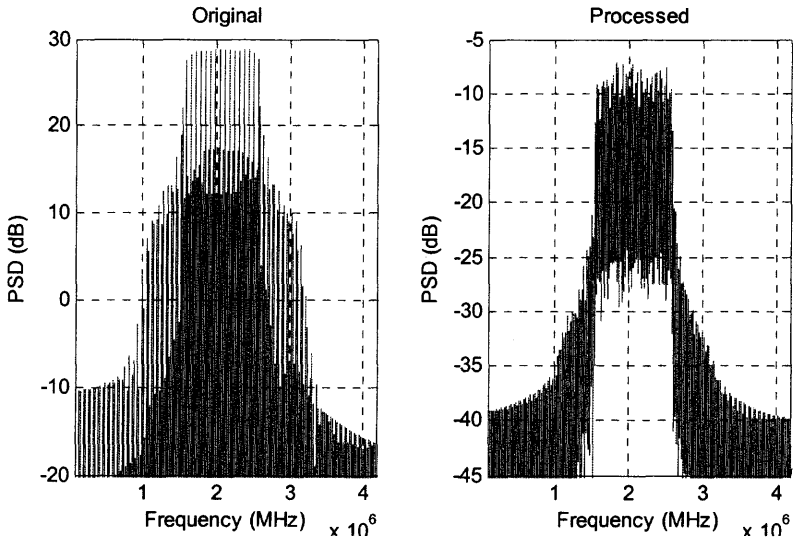

Figure 3.12 Comparison of RFR (a) original scrambler and (b) LFSR-28 & new 4-seed & with RFR.

Simulation is conducted and results are shown in Figure 11 and 12. In Figure 11, same configuration as in sub-section 3.2.1 and 3.2.2 is used. Payload data are all "1"s to the scrambler and non-payload data takes about 3.1%. In Figure 11, (a) is PSD of data processed by original scrambler, or LFSR-15 with four seeds, and (b) PSD of data processed by LFSR-15 with new four seeds and RFR. In Figure 12, (a) is PSD of data processed by current scrambler, i.e., LFSR-15 with four seeds, and (b) PSD of data processed by proposed scheme, i.e., LFSR-28 using new four seeds and with RFR. The new four seeds are generated by MATLAB rand() function. Results in Figure 11-(b) and 12-(b) showed that the new scheme reduces the PSD of UWB signals significantly, about 34 dB and 37dB respectively over current PHY.

3.4 Conclusion

In this chapter, it is observed that lines in spectrum are still an issue for MB-OFDM UWB signals. A mechanism in base-band processing to remove lines in spectrum, therefore to reduce the peak value of the PSD of MB-OFDM UWB signals was proposed. Furthermore a new scrambler to reduce the peak value of the PSD of MB-OFDM UWB systems used in IEEE 802.15.3a. Simulations show that the proposed approach is effective in suppressing the PSD of MB-OFDM UWB signals. In addition, it satisfies the important practical criteria of being both simple and easy to implement.

CHAPTER 4

ITERATIVE CODES GENERATION FOR SYNCHRONOUS DS-MULTIBAND OFDM SYSTEM

Multiband OFDM, considered in the previous chapters, is a new modulation scheme which evolved in March 2003 to expedite the process of time to market of this technology as well as to overcome the existing limitations in the current silicon technology for handling short baseband pulses of order of nanoseconds by UWB that spreads the energy over a large bandwidth thereby requiring proportionately large Rake fingers. The primary purpose being, to split the entire spectrum into 528 MHz wide sub-bands and further use OFDM to overcome frequency selectivity of the channel thereby eliminating multipath. The reason for using the multiband solution over single sub-band owes to meeting the requirement of 10 m range as set by FCC.

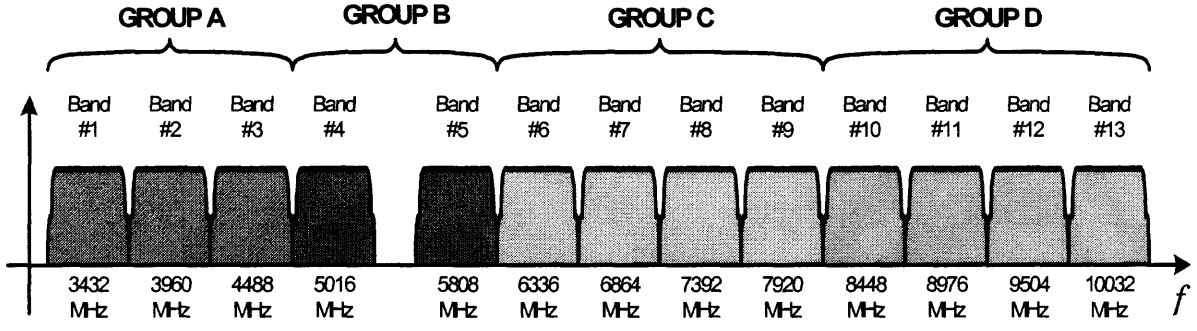

Figure 4.1 Multiband spectrum groups of UWB.

Under this new scheme, it was proposed that 128 sub-carriers OFDM symbol will be transmitted by the piconets in a repeated fashion 1 2 3 or 1 3 2 etc. in the three sub-bands to be used initially. The cyclic prefix is used at the beginning of each OFDM symbol and a guard interval of 9.5 ns is added to each OFDM symbol, which ensures that

only a single RF transmit and receive chain are required for all channels and data rates while the transmitter and receiver have adequate time to switch to the next channel.

Wireless Home is one of the long term goals envisioned by wireless industry and MB-OFDM is set to play an important role in achieving it. In such a setup, large number of electronic devices ranging from fax, printers, etc. to refrigerators, microwaves, thermostats etc. will be operating in close proximity thereby contributing to large interference. The current scheme of Multiband – OFDM proposed in IEEE 802.15.3a committee restricts the capacity to three as seen clearly in Figure 3 and is hence incapable of meeting such a demand.

It is shown in this chapter that in order to enhance user capacity, constrained as a result of the proposed transmitted scheme of OFDM symbol as well as lack of robustness and protection for unsynchronized users, a synchronous OFDM system with single or multiple codes assigned per piconet/user is a viable solution. Such a network is shown to scale the number of users while keeping the interference under control and maintaining the high data rates. Also an architecture encompassing central controller for purpose of co-ordination has been proposed. A system parallel to CAHAN (Cellular Ad Hoc Network) is considered but at a micro level, which is assumed to allow peer to peer communication under limited interference and hence smaller number of users, and controlled communication through this central controller when large number of users are in the system. The technique also offers flexibility in assigning code corresponding to each OFDM subcarrier frequency depending upon the extent of flat fading. In other words, channels experiencing deep fades can be assigned codes accordingly to overcome

the fading effect. Uplink between the communicating devices and the central controller is considered and addressed in this chapter.

Section 4.1 proceeds with signal model which leads the discussion into problem formulation and possible central controller receiver structure in Section 4.2- Section 4.5. In Section 4.4 an architecture consisting of iterative code generation unit along with scheme of using the codes is proposed for user capacity enhancement of the system while maintaining simplicity in design.

4.1 Signal Model

Consider symbol synchronous Multiband OFDM system with K users. Let T be the duration of each OFDM symbol transmitted. The symbols are transmitted in both time and frequency slots as shown below in Figure 4.2. The number of available slots (frequency & time) determines the number of piconets that can be accommodated by such a system. The symbol power in each of the slots is therefore multiplied by certain factors, which in totality, over all the frequency time slots, forms a code. In other words each of these coded symbols, transmitted in different slots, is collected at the receiver and then decoded to obtain the actual symbol transmitted. Such a code, spread in frequency and time is used to distinguish between different users.

Let $s_j(t)$ be the OFDM symbol transmitted by the j^{th} user $\forall t \in (0,T)$. Let the multipath channel $h(t)$ be confined to finite interval $[0,T_b]$. From [15], let the sequence $h_0\, h_1 \ldots\ldots h_u$ denote the baseband equivalent impulse response of the channel sampled at the rate $1/T_s$, with

$$T_b = (1+\nu)T_s \tag{4.1}$$

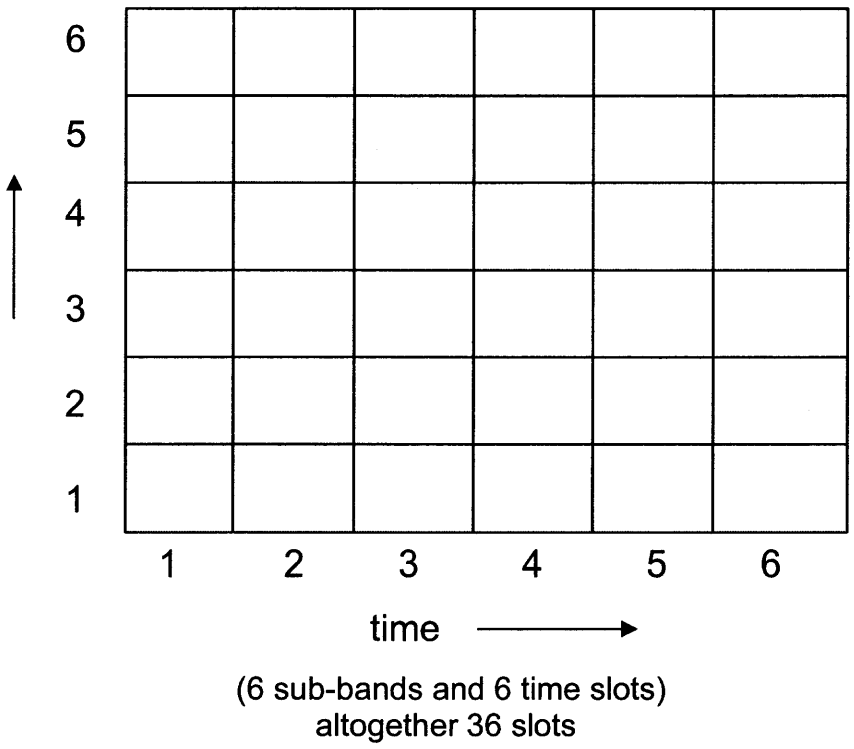

Figure 4.2 Grid showing the time frequency slots, with time slots along x-axis and frequency slots along y-axis.

To continue with the discrete description of the system, let $s_j[n] = s_j(nT_s)$ and $w_j[n] = w_j(nT_s)$ denote samples of transmitted symbol and the sample of channel noise for the j^{th} user respectively. To overcome the effect of intersymbol interference a cyclically extended guard interval is created which converts the linear convolution of symbol and channel into a circular convolution. Let the code for the j^{th} user that is used to hide these symbols from others be given by c_j.

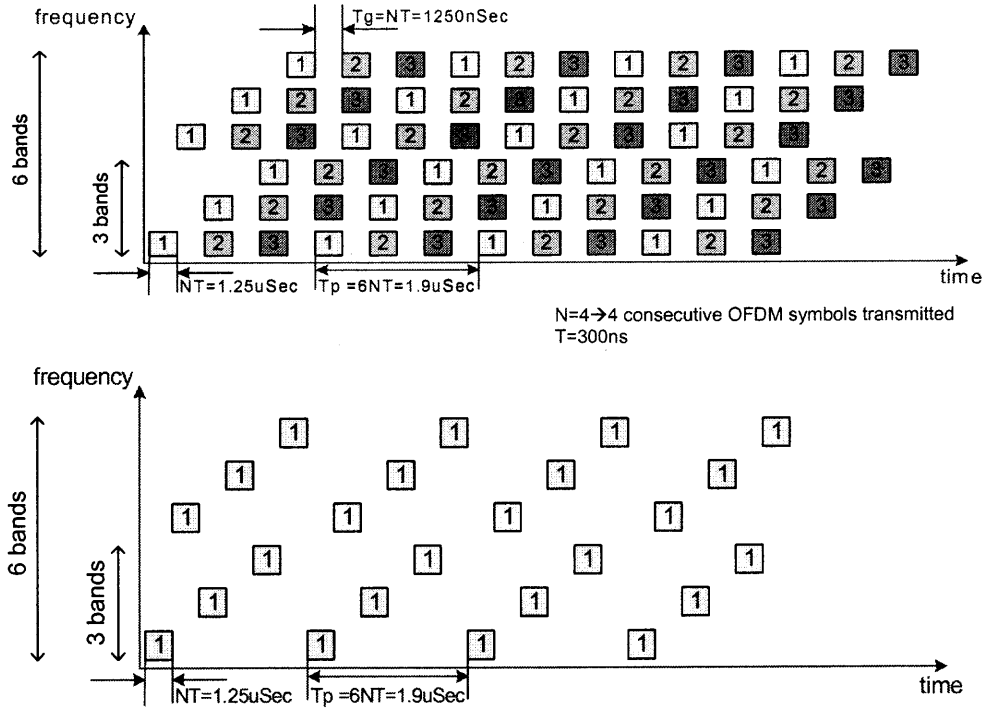

Figure 4.3 Transmission hopping sequence in a synchronous MB-OFDM as proposed by Infineon in a presentation [9] before IEEE 802.15.3a committee. The user capacity is restricted to 3.

With everything in place including the cyclic prefix, the matrix description of the channel as seen by the j^{th} user is as follows:

$$y_j = H_j c_j s_j \tag{4.2}$$

where,

$$H_j = [H_{j1}\, H_{j2} \ldots . H_{jN_v}] \qquad \forall N_v = N_f N_t \tag{4.3}$$

where N_f is the number of frequency slots

N_t is the number of time slots

$$H_{jk} = \begin{bmatrix} h_{j0}^k & h_{j1}^k & h_{jl}^k & \cdots & h_{jv}^k & 0 & \cdots & 0 \\ 0 & h_{j0}^k & h_{j1}^k & \cdots & h_{j(v-1)}^k & h_{jv}^k & \cdots & 0 \\ \vdots & \vdots & \vdots & & \vdots & \vdots & & \vdots \\ h_{j1}^k & h_{j2}^k & h_{j3}^k & \cdots & h_{jv}^k & 0 & \cdots & h_{j0}^k \end{bmatrix} \tag{4.4}$$

h_{jl}^k is the l^{th} channel sample in the k^{th} slot of the j^{th} user.

$$\mathrm{c_j} = [c_{j1}\, c_{j2} \ldots . c_{jN_v}]^T \tag{4.5}$$

is the initial code vector spanning the entire time-frequency space for a single symbol.

$$c_{jk} = \alpha_{jk} \mathrm{I}_N \qquad \forall \alpha_j^T \alpha_j = 1 \tag{4.6}$$

$$\mathrm{s_j} = [s(N-1)\; s(N-2) \ldots . s(0)]^T \times 1_{\mathrm{N_v}} \tag{4.7}$$

Therefore, the transmitted symbol can be written as

$$\mathrm{y_j} = \left(\sum_k H_{jk} c_{jk} \right) \mathrm{s_j} \tag{4.8}$$

Now let, X be the received signal then,

$$\mathrm{x} = \sum_{j=1}^{\mathrm{K}} \mathrm{y_j} + \mathrm{w} \tag{4.9}$$

The discrete Fourier transform of N-by-1 vector X is defined by the N-by-1 vector

$$\mathrm{X} = [X[N-1], X[N-2], \ldots., X[0]] \tag{4.10}$$

where

$$X(k) = \frac{1}{\sqrt{N}} \sum_{n=0}^{N-1} x[n] \exp\left(-j \frac{2\pi}{N} kn \right), \qquad k = 0,1,\ldots\ldots,N-1 \tag{4.11}$$

The exponential term is referred to as kernel of DFT. Correspondingly, the inverse discrete Fourier transform (IDFT) of the N-by-1 vector X is defined by

$$x[n]=\frac{1}{\sqrt{N}}\sum_{k=0}^{N-1}X[k]\exp\left(j\frac{2\pi}{N}kn\right), \qquad n=0,1,.....,N-1 \qquad (4.12)$$

Equations (4.5) and (4.6) are also known as *analysis* and *synthesis* equations respectively An important property of circulant matrix exemplified by the channel matrix H_{jk} is that it permits spectral decomposition

$$H_{jk}=Q^{H}\Lambda_{jk}Q \qquad (4.13)$$

where H in subscript stands for Hermitian transpose. The matrix Q is a square matrix defined in terms of kernel of N-point DFT as follows:

$$Q=\begin{bmatrix} \exp\left(-j\frac{2\pi}{N}(N-1)(N-1)\right) & \cdots & \exp\left(-j\frac{2\pi}{N}2(N-1)\right) & \exp\left(-j\frac{2\pi}{N}(N-1)\right) & 1 \\ \exp\left(-j\frac{2\pi}{N}(N-1)(N-2)\right) & \cdots & \exp\left(-j\frac{2\pi}{N}2(N-2)\right) & \exp\left(-j\frac{2\pi}{N}(N-2)\right) & 1 \\ \vdots & & \vdots & \vdots & \vdots \\ \exp\left(-j\frac{2\pi}{N}(N-1)\right) & \cdots & \exp\left(-j\frac{2\pi}{N}2\right) & \exp\left(-j\frac{2\pi}{N}\right) & 1 \\ 1 & & 1 & 1 & 1 \end{bmatrix} \qquad (4.14)$$

From the above it is clear that the k^{th} element of the N-by-N matrix, Q, starting from the bottom right at $k=0$ and $l=0$ and counting up step by step is

$$q_{kl}=\frac{1}{\sqrt{N}}\exp\left(-j\frac{2\pi}{N}kl\right), \qquad (k,l)=0,1,.....,N-1 \qquad (4.15)$$

The matrix Q is a unitary matrix i.e.

$$Q^H Q = \mathrm{I} \tag{4.16}$$

where I is the identity matrix.

The matrix Λ_{jk} is a diagonal matrix that contains the N discrete Fourier transform values of the sequences $h_0\, h_1 \ldots\ldots h_u$ characterizing the channel.

$$\Lambda_{jk} = \begin{bmatrix} \lambda_{jN-1}^{k} & 0 & \cdots & 0 \\ 0 & \lambda_{jN-2}^{k} & \cdots & 0 \\ \vdots & \vdots & & \vdots \\ 0 & 0 & & \lambda_{j0}^{k} \end{bmatrix} \tag{4.17}$$

4.2 Receiver

When a receiver receives the transmitted signal, the modulated passband data is converted into baseband by process of demodulation. At this point the transmitted symbols are made to pass through DFT block, after having removed the cyclic prefix and hence the effect of multipath. Using the orthonormal matrix Q for recovering the original data shows the demodulation process. As shown in [15] again, if the received signal vector is X then,

$$\mathrm{X} = Q\mathrm{x} \tag{4.18}$$

From equations (4.9) and (4.18)

$$\mathrm{X} = Q\left(\sum_{j=1}^{\mathrm{K}} \mathrm{y_j} + \mathrm{w}\right) \tag{4.19}$$

From equations (4.2) and (4.8)

$$y_j = H_j c_j s_j = \left(\sum_{k=1}^{N_v} H_{jk} c_{jk} \right) s_j$$

On substituting the above expression in (4.19) following is obtained,

$$X = Q\left(\sum_{j=1}^{K} \left(\sum_{k=1}^{N_v} H_{jk} c_{jk} \right) s_j + w \right)$$

$$\Rightarrow \qquad X = \sum_{j=1}^{K} \sum_{k=1}^{N_v} Q H_{jk} c_{jk} s_j + Q w \tag{4.20}$$

Using relations (4.6) & (4.13) in the above expression,

$$X = \sum_{j=1}^{K} \sum_{k=1}^{N_v} Q Q^H \Lambda_{jk} Q \alpha_{jk} I_N s_j + Q w \tag{4.21}$$

which finally leads to

$$X = \sum_{j=1}^{K} \sum_{k=1}^{N_v} \alpha_{jk} \Lambda_{jk} S_j + W \tag{4.22}$$

where

$$S_j = Q s_j$$

Decomposing expression (4.22) into its constituent elements

$$X[p] = \sum_{j=1}^{K} \sum_{k=1}^{N_v} \alpha_{jk} \lambda_{jp}^{k} S_j[p] + W[p] \qquad p = 0,1,....,N-1 \tag{4.23}$$

The above equation suggests N-parallel CDMA type transmission. Now if the number of users/piconets $K > N_v$, then the system is considered to be overloaded. On the other hand, if $K < N_v$ then the system is underloaded. It can be easily seen that in an

overloaded system the user transmission shall cease to be orthogonal. As will be shown later, the receiver which will aid in co-ordination and synchronization along with host of other operations, will also help in decoding each of the sent data and transmit it further to final destination. This receiver is therefore modeled along the same lines as the base unit of a cordless phone. For decoding purposes only the final code matrix containing the code of each user in the system that will embody MMSE functionality (Figure 4.5) will be placed on this central controller overlooking the communication in the Personal Area Network (PAN). By shifting the brunt of computation onto this central receiver, the design of mobile and other communicating devices for such a short range wireless communication can be kept simple. In essence this multi-access technique is very similar to Bluetooth Master/Slave configuration, only difference being that in the proposed technique there is a universal Master (central receiver) while all the other communicating devices are Slaves.

4.3 Welsh Bound and Total Squared Correlation

Welsh derived a lower bound for maximum correlation [10] among K users having unit energy sequences as

$$\sum_{i=1}^{K}\sum_{j=1}^{K}\left(\beta_i^T\beta_j\right)^2 \geq \frac{K^2}{N_v} \tag{4.24}$$

where, $\beta_i, i=1,...,K$, are the signature sequences of the K users.

The LHS in the above expression is commonly referred to as Total Squared Correlation (TSC). When $K < N_v$ then TSC=K which is achieved by K orthonormal vectors. On the other hand, when $K > N_v$, the Welsh bound can be achieved. It has been

shown [11] that the set of signature sequences meeting Welsh bound satisfy following property

$$\beta^T\beta = \frac{K}{N_v}\mathrm{I}_{N_v} \qquad \text{for the case when} \qquad K > N_v \qquad (4.25)$$

$$\beta^T\beta = \mathrm{I}_K, \qquad \text{for the case when} \qquad K < N_v \qquad (4.26)$$

However the number of users that can be admitted into this overloaded system is upper bounded [14] by $K < N_v(1+1/\mu)$

$$K < N_v(1+1/\mu) \qquad (4.27)$$

where μ is SIR threshold. Assume that $\beta_i, i = 1,...,K$, are the signature sequences of the users. Also let us assume that the signals are received at the central controller with all signal processing capabilities (similar to base station in cellular network) by matched filters, and transmitted power for all users is assumed to be same i.e. $p_i = p$ .If the received signal is **r** then the MSE for the i^{th} user is [4]

$$\mathrm{MSE}_i = E\left[\left(\mathrm{r}^T\beta_i - s_i\right)^2\right] \qquad (4.28)$$

$$= \beta_i^T\left(p\sum_{j=1}^{K}\beta_j\beta_j^T + \sigma^2\mathrm{I}_{N_v}\right)\beta_i - 2\sqrt{p}\beta_i^T\beta_i + 1 \qquad (4.29)$$

The total MSE in the system will be

$$\mathrm{MSE} = \sum_{i=1}^{K}\mathrm{MSE}_i \qquad (4.30)$$

$$= p\sum_{i=1}^{K}\sum_{j=1}^{K}\left(\beta_i^T\beta_j\right)^2 - \left(2\sqrt{p} - \sigma^2\right)\sum_{i=1}^{K}\beta_i^T\beta_i + K \qquad (4.31)$$

Observing that the first term in equation (4.31) is nothing but TSC from equation (4.24) and making use of the fact that the signature sequences are unit energy vectors

$$\text{MSE} = p\text{TSC} + \left(1 + \sigma^2 - 2\sqrt{p}\right) + K \tag{4.32}$$

Equation (4.32) shows direct relationship between MSE and TSC. It therefore implies that MSE of the system can be decreased by correspondingly reducing the TSC.

$$\text{TSC} = \left(\beta_k^T \beta_k\right)^2 + 2\beta_k^T \left(\sum_{j \neq k} \beta_j \beta_j^T\right) \beta_k + \gamma_k \tag{4.33}$$

where

$$\gamma_k = \sum_{i \neq k} \sum_{j \neq k} \left(\beta_i^T \beta_j\right)^2 \tag{4.34}$$

Since all signature sequences are assumed to be unit energy vectors, equation (4.33) reduces to

$$\text{TSC} = 2\beta_k^T A_k \beta_k + \gamma_k + 1 - 2\sigma^2 \tag{4.35}$$

where

$$A_k = \sum_{j \neq k} \beta_j \beta_j^T + \sigma^2 \mathrm{I}_{N_v} \tag{4.36}$$

4.4 TSC Reduction & Iterative Algorithm

In [12] it was proposed that if k^{th} user's sequence is replaced with following

$$c_k = \frac{A_k^{-1} \beta_k}{\left(\beta_k^T A_k^{-2} \beta_k\right)^{1/2}} \quad \text{where} \quad c_k^T c_k = \beta_k^T \beta_k = 1 \tag{4.37}$$

then the new set of sequences is given by

$$\overline{\beta} = \left[\beta_1 \cdots \beta_{k-1}\ c_k\ \beta_{k+1} \cdots \beta_K\right] \tag{4.38}$$

As can be seen c_k is normalized MMSE filter for user k. MMSE filter can be regarded as special matched filter which bears lower cross correlation with signature sequences of different users. The revised TSC is now given as,

$$\mathrm{TSC}_{new} = 2\frac{\beta_k^T A_k^{-1} \beta_k}{\beta_k^T A_k^{-2} \beta_k} + \gamma_k + 1 - 2\sigma^2 \tag{4.39}$$

In [Appendix A, 12] it is shown that $\mathrm{TSC}_{new} \leq \mathrm{TSC}_{old}$ where equality holds when $c_k = \beta_k$ .Based on above, they proposed an iterative algorithm whereby each user updated its sequence in a sequential manner until unless no further reduction in TSC is possible i.e. the algorithm converges [Section IV, 12].

4.5 Proposed System

Taking cue from Ulukus and Yates iterative algorithm for constructing optimum signature sequence sets in a synchronous CDMA type environment, it is proposed to use the same algorithm in synchronous Multiband–OFDM system introduced in the earlier sections. Recalling our final expression (4.23) which decomposed the system into N-parallel CDMA systems, each such system can strive for optimality by using the iterative algorithm and simultaneously updating each sequence corresponding to the seemingly independent parallel channels in an equally independent fashion. Therefore, there will be N-simultaneous systems which will undergo this process of iterative updates based on TSC reduction at each stage, Figure 2.

$$X[p] = \sum_{j=1}^{K} \sum_{k=1}^{N_v} \alpha_{jk} \lambda_{jp}^{k} S_j[p] + W[p] \qquad p = 0,1,\ldots,N_v - 1$$

Now putting $\beta_{jk}^{p} = \alpha_{jk}\lambda_{jp}^{k}$ in the above expression

$$X[p] = \sum_{j=1}^{K}\sum_{k=1}^{N_v}\beta_{jk}^{p}S_j[p] + W[p] \tag{4.40}$$

Therefore code sequence for the p^{th} data channel corresponding to j^{th} user will be

$$\beta_j^p = \left[\beta_{j1}^p, \ldots, \beta_{jN_v}^p\right] \tag{4.41}$$

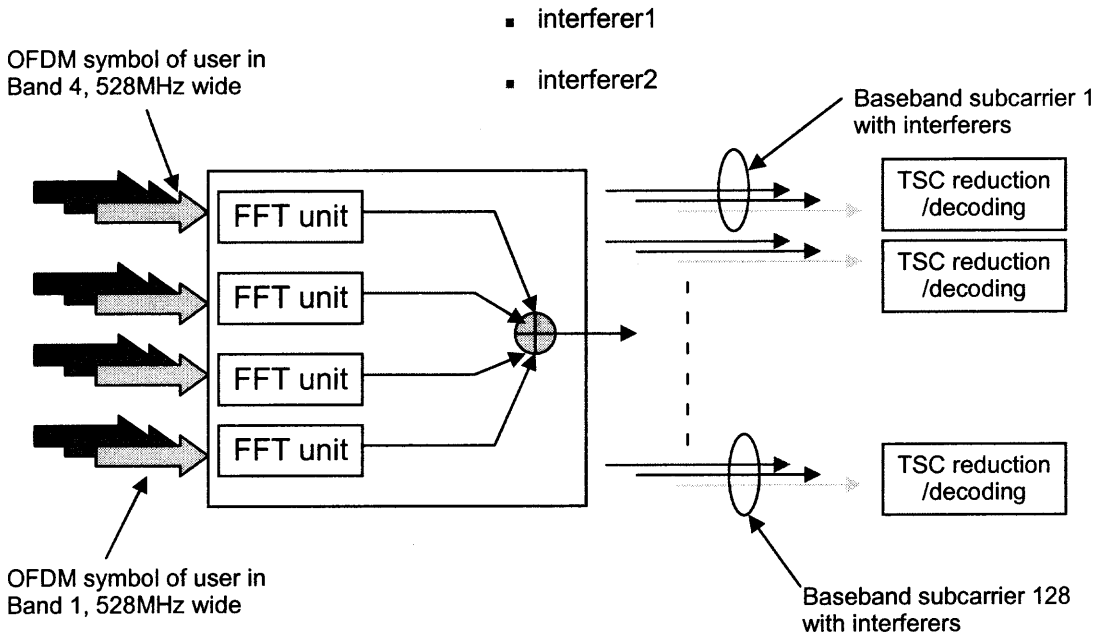

Figure 4.4 Shows simplified receiver structure. The incoming signal modulated to occupy different bands contains interfering signals of other users. This signal is fed to FFT block which has added functionalities than simply performing FFT operation. Output of the receiver contains 128 baseband subcarrier signals which are to be treated independently. Initially the receiver generates adhoc codes through TSC reduction mechanism which are fed back to transmitters. Eventually, each subcarrier allows for CDMA like processing/decoding.

Now each of these β_j^p for each of the K users and each of the N- channels has to be optimized to achieve the lowest TSC which is which is lower bounded by equation

(4.24). Although convergence always exists, but as shown by the same authors in [13], there also exists suboptimal solution of the fixed points (the final signature set of each user).

But if the initial sequence is randomly chosen then the simulations show always a convergence to the optimal set of fixed points.

Intuitively, if the sequences are completely randomly chosen then the choice of update i.e. at a given time which one of the users whose sequence remains to be updated, is updated would affect the convergence. Recalling equation (4.39),

$$\mathrm{TSC}_{new} = 2\frac{\beta_k^T A_k^{-1} \beta_k}{\beta_k^T A_k^{-2} \beta_k} + \gamma_k + 1 - 2\sigma^2$$

Now, updating the user whose update results in greater reduction of TSC should lead to faster convergence towards the lower bound in equation (4.24). Therefore the user to be updated should be chosen according to the following parameter,

$$\min \mathrm{TSC} \tag{4.42}$$

$$\Rightarrow \quad \min\left(2\frac{\beta_k^T A_k^{-1} \beta_k}{\beta_k^T A_k^{-2} \beta_k} + \gamma_k \right) \tag{4.43}$$

Therefore user k will be updated before remaining users provided

$$2\frac{\beta_k^T A_k^{-1} \beta_k}{\beta_k^T A_k^{-2} \beta_k} + \gamma_k \le 2\frac{\beta_j^T A_j^{-1} \beta_j}{\beta_j^T A_j^{-2} \beta_j} + \gamma_j \qquad \begin{matrix} (j,k) \in (\bar{K},\ldots,K) \\ \forall j \in (\bar{K},\ldots,K) \end{matrix} \tag{4.44}$$

where $\bar{K}$ -1 are the number of users already updated

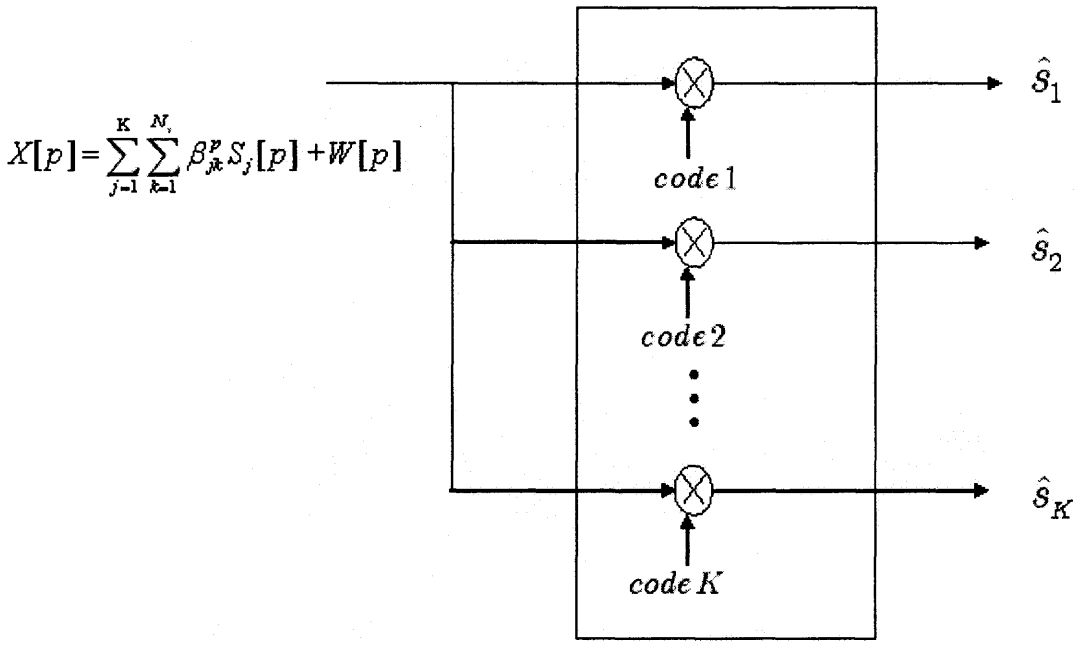

Figure 4.5 Receiver operation once the codes have been generated and assigned to the users. A simple decoding scheme whereby the received signal is multiplied by the respective codes of the users which are in essence performing the MMSE operation as can be seen from (44).

Simplifying (46) using linear algebra yields the following final expression,

$$\min\left(\left(\frac{\beta_k^T A_k^{-1}\beta_k}{\beta_k^T A_k^{-2}\beta_k}\right)-\sum_{j\neq k}\left(\beta_j^T\beta_k\right)^2\right) \qquad \forall k\in(\bar{K},\ldots,K) \qquad (4.45)$$

The signal adaptation algorithms operate slowly as compared to those for multiuser interference suppression. Therefore, such a procedure shall be appropriate for a stable channel which for the case of indoor channel is a reasonable assumption.

The computations here is assumed to be performed by central controller which aids in co-ordination and overseeing the communication process involving synchronization, channel estimations, code generation, code assignment and power transmission control (within FCC regulation).

4.6 Simulation

Simulations were performed for a number of different cases, but the results shown here is subset of those cases. One case is cited here. For obtaining the sequences, IEEE 802.15.3a UWB channel type 2 (NLOS 4 - 10m) were used. Channel impulse responses corresponding to different channels (1000 channels obtained) were generated and allotted to each user for transmission in different frequency bands. Channel impulse responses corresponding to a single subcarrier class in each frequency band was then considered, like for instance subcarrier 1 in band 1, band 2, band 3 so and so forth, for all the users and iterative TSC reduction MMSE algorithm was applied to obtain the final sequences as well as the power to be allocated to the given subcarrier under consideration in different frequency bands. In order to circumvent allocation of large power for the channel in deep fade a simple power threshold was used in simulation to distribute the channel energy in other dimensions. Following tables show the code sequences and the normalized power which each user puts on the given subcarrier.

Case : $N_v = 9,\ K = 10$

The following table contains the code for the 10 users at the transmitter sides.

Table 4.1 Codes for Coding the User Data at Transmitter Side

code1	-0.07011	0.41067	-0.62808	-0.67454	-0.09687	0.030742	0.06029	-0.94136	-0.53269
code2	-0.10877	0.16633	0.93579	-0.09063	0.5876	-0.28132	0.020508	-0.40591	-0.40667
code3	0.25733	0.27074	0.097551	0.51912	0.069651	-0.20258	-0.21639	0.65681	-0.64744
code4	-0.41948	0.2941	0.21528	-0.0801	0.50562	0.84403	-0.26525	-0.74928	-0.79075
code5	-0.35121	-0.41034	-0.09994	0.2732	0.38074	-0.93628	0.31375	0.31994	-0.23184
code6	-0.82017	-0.2	-0.91149	0.046573	0.10761	-0.28645	-0.92507	-0.15111	0.38049
code7	-0.27305	0.43259	0.92707	0.085158	-0.1356	-0.35151	0.36296	-0.08447	0.23868
code8	-0.26185	0.27633	-0.2375	0.11262	0.061447	0.18434	-0.42181	0.87519	0.78042
code9	-0.27203	0.48945	0.20426	-0.2794	-0.17265	-0.22001	-0.21029	0.41562	-0.31955
code10	0.13895	0.011701	-0.21774	-0.19344	0.23463	0.175	0.15251	0.22372	0.31796

The following code is at the receiver side (central controller) after the signals pass through the channel.

Table 4.2 Codes at the Receiver Side

code1	-0.03592	0.5488	-0.63801	-0.16507	-0.24898	0.046559	0.1457	-0.3737	-0.19539
code2	-0.15636	0.26007	0.17968	-0.07752	0.60496	-0.39316	0.021782	-0.38029	-0.45164
code3	0.49629	0.34023	0.10722	0.6079	0.086571	-0.13346	-0.32611	0.23473	-0.26485
code4	-0.23699	0.0083	0.4005	-0.07656	0.092591	0.68074	-0.38691	-0.35299	-0.17671
code5	-0.5571	-0.44038	-0.20115	0.41336	0.043952	-0.08764	0.24801	0.14988	-0.43679
code6	-0.11275	-0.25947	-0.15418	0.059979	0.1139	-0.48914	-0.49358	-0.41375	0.47492
code7	-0.2331	0.37794	0.52485	0.17664	-0.04861	-0.16072	0.54549	-0.08545	0.40386
code8	-0.59102	0.45266	-0.19927	0.26119	0.071275	0.12757	-0.36124	0.33389	0.27303
code9	-0.19806	0.13206	0.21425	-0.61873	-0.15169	-0.35818	-0.25693	0.49435	-0.23
code10	0.13025	0.005246	-0.27305	-0.21385	0.78849	0.23625	0.18486	0.30052	0.24635

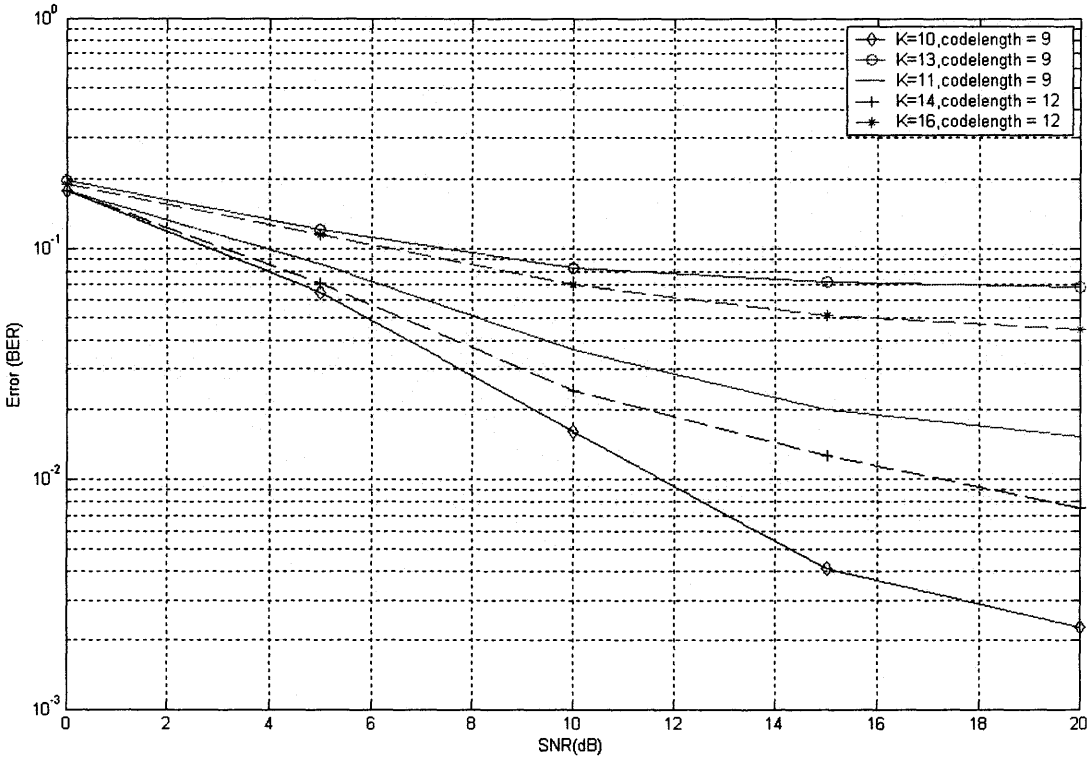

Figure 4.6 Comparison of BER for different number of users in the system K=10, 11 & 13 with code lengths (N_v)=9 and for K=14 & 16 when a single frequency subband is added and the code length is increased to 12.

CHAPTER 5

PERFORMANCE AGAINST INTERFERENCE

The proposed scheme of communication discussed in Chapter 4 involving iteratively generated codes for each active user in the PAN system for user capacity enhancement, needs to be analyzed for performance in presence of interference. This chapter takes a look at this feature where performance of the system in presence of interference co-existing in the operational band is considered. The effect of interference is also analyzed by observing its possible effect on the user capacity.

One of the key features of UWB, of it occupying a very large bandwidth, required that it should not cause any unnecessary interference to the existing narrowband (NB) technologies present in certain portions of the operational bandwidth. As a result, FCC imposed power constraints to check the interference from UWB to NB systems. However it's the reverse situation that is more problematic. The interference due to narrowband systems on the UWB can be overwhelming. First, the total power of a NB transmission generally will fall within the UWB passband. Second, a wide UWB passband (several hundred MHz or more) may span multiple NB transmitters, some of which may be very powerful and/or very near to the UWB receiver. This was one of the reasons which led to single band UWB giving way to Multiband approach. This split the UWB's 7.5 GHz band into 14 multibands each spanning 528 MHz as shown in Figure 4.1.. This meant that the band which had tremendous presence of narrowband systems could be shut off thereby causing no interference or experiencing interference in return.

However, multiband approach does not completely solve the problem at hand. The Multibands themselves span over hundreds of MHz and pose similar problem as its parent single band yet again. The combination of Multiband with OFDM which was proposed by Texas Instruments, aimed at effectively handling the multipath as well as narrowband interference issues. With OFDM splitting the broad frequency selective channel into several narrowband frequency flat channels, the NB interference would now affect the tones (approx. 4 MHz wide) and hence, the data carried by those tones simply. The narrowband interference would therefore affect some of the tones thereby rendering the information on these tones unreliable. One can then employ error correction techniques like FEC as proposed by the MBOA to recover the lost data. This chapter considers the system proposed in the previous section and analyzes its behavior in presence of narrowband interference. It will be seen that the system adapts well to such interference and when error correction techniques are incorporated alongside the performance can be further improved.

5.1 Types of Interference

There are primarily two types of interference considered here:

(i) Constant interference: Such an interference can be present within a narrowband at all times. It could be due to microwave devices which are on for large chunk of time. Such interference can be known precisely at the central controller.

(ii) Narrowband Interference: Interference due to other narrowband technologies like 802.11a etc. of which only the amount of power put out within the band can be known.

The approach for handling the two types of interference defined above is different. Constant interference shall be first considered for analysis.

5.1.1 Constant Interference

As mentioned above, the constant interference can be known precisely at the central receiver. Let us assume the presence of such interference in one of the tones. From expression (4.3), the received signal at the central controller in presence of a constant interference in one of the tones, say l^{th} tone, is given by

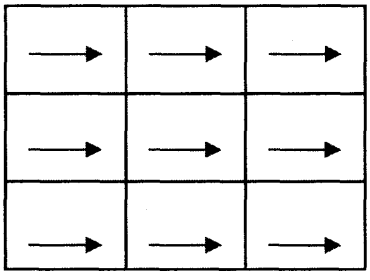

Figure 5.1 A given sub-carrier spread along the time-frequency grid.

$$X[l] = \sum_{j=1}^{K} \sum_{k=1}^{N_v} \beta_{jk}^{l} S_j[l] + W[l] + I \tag{5.1}$$

where I represents the interference. Now assuming this interference is known precisely at the receiver since its constant, the interference can be treated as another virtual user in the system with different amount of power. As a result the number of users in such a system is K+1. Dropping the subscript l and replacing the summation in equation (5.1) by the vector product. From equation (4.9), the minimum square error for i^{th} user is

$$\mathrm{MSE}_i = \beta_i^T \left(p \sum_{j=1}^{K} \beta_j \beta_j^T + p_{K+1} \beta_{K+1} \beta_{K+1}^T + \sigma^2 \mathrm{I}_{\mathrm{N_v}} \right) \beta_i - 2\sqrt{p} \beta_i^T \beta_i + 1 \tag{5.2}$$

where, interference I is represented by a code vector β_{K+1} and p_{K+1} is the interference power. The total MSE of the system is then given by

$$\mathrm{MSE} = \sum_{i=1}^{K} \mathrm{MSE}_i$$

$$= p\sum_{i=1}^{K}\sum_{j=1}^{K}\left(\beta_i^T\beta_j\right)^2 + p_{K+1}\sum_{i=1}^{K}\left(\beta_i^T\beta_{K+1}\right)^2 - \left(2\sqrt{p}-\sigma^2\right)\sum_{i=1}^{K}\beta_i^T\beta_i + K \tag{5.3}$$

Representing the total MSE in terms of Total Squared Correlation similar to the expression in (4.32),

$$\mathrm{MSE} = p\mathrm{TSC} + \left(1+\sigma^2-2\sqrt{p}\right)K \tag{5.4}$$

Therefore,

$$\mathrm{TSC} = \sum_{i=1}^{K}\sum_{j=1}^{K}\left(\beta_i^T\beta_j\right)^2 + \frac{p_{K+1}}{p}\sum_{i=1}^{K}\left(\beta_i^T\beta_{K+1}\right)^2$$

$$= \left(\beta_m^T\beta_m\right)^2 + 2\beta_m^T\left(\sum_{j\neq m}\beta_j\beta_j^T\right)\beta_m + \frac{p_{K+1}}{p}\beta_m^T\left(\beta_{K+1}\beta_{K+1}^T\right)\beta_m + \gamma_m \tag{5.5}$$

where, γ_m is the same as defined in expression (4.34). The above expression shows the role of each user, in this case m^{th} user, in the Total Squared Correlation. Finally,

$$\mathrm{TSC} = 2\beta_m^T A_m \beta_m + \gamma_m + 1 - 2\sigma^2 \tag{5.6}$$

where,

$$A_m = \sum_{j\neq k}\beta_j\beta_j^T + \frac{p_{K+1}}{2p}\left(\beta_{K+1}\beta_{K+1}^T\right) + \sigma^2\mathrm{I}_{\mathrm{N_v}} \tag{5.7}$$

As can be readily observed, the expression for TSC with constant interference is the similar to that obtained without any narrowband interference. Consequently, same iterative procedure for reduction of TSC is followed until it converges. The codes therefore adapt in such an interfering environment thereby providing extra protection against interference.

5.1.2 Unknown Narrowband Interference

Incase of unknown NB interference, where the exact signal may not be known precisely, but for the actual power in the interfering band one can easily deduce the expression for TSC given below

$$\mathrm{TSC} = 2\beta_m^T A_m \beta_m + \gamma_m + 1 - 2\sigma^2$$

where,

$$A_m = \sum_{j \neq k} \beta_j \beta_j^T + \sigma^2 \mathrm{I}_{\mathrm{N}_v} + \sigma_I^2 \mathrm{G}_{\mathrm{N}_v} \tag{5.8}$$

σ_I^2 is the interference power and $\mathrm{G}_{\mathrm{N}_v}$ is a square matrix ($\mathrm{N}_v \times \mathrm{N}_v$) with diagonal elements showing the presence of interference in different time frequency slots. In worst case scenario, if the interference is present in all time frequency slots then $\mathrm{G}_{\mathrm{N}_v} = \mathrm{I}_{\mathrm{N}_v}$ i.e is an identity matrix.

5.2 Effect on User Capacity of NB interference

The effect of NB interference on user capacity of the system shall be evaluated in this section. In Chapter 4, an expression (4.27) provided the number of users that can be admitted into the system based on desirable SINR. This expression which was derived in [14] is a very general expression without taking into consideration any power constraints. However in [14], authors later to derive the expression for the upper bound on the user capacity with power constraint. Following the same direction in deriving capacity upper bound, the effect of NB noise on the system user capacity is observed. For deriving the upper bound on user capacity, simply consider a single subcarrier in all the slots.

Recalling the overall channel model for a subcarrier in all the slots

$$Y = \beta S + W \tag{5.9}$$

where β is the code vector, S is the transmitted symbol and W is the noise vector.

If $\hat{S}$ is the MMSE estimate of transmitted symbol S, then direct application of orthogonality principle yields

$$\hat{S} = D\beta^T \left(\beta D\beta^T + \sigma^2 I_{N_v}\right)^{-1} Y \tag{5.10}$$

where D is a diagonal matrix with fixed user powers as diagonal entries and hence is the covariance matrix of S. The covariance matrix of the error $\in = S - \hat{S}$ is given by

$$K_{\in} = D - D\beta^T \left(\beta D\beta^T + \sigma^2 I_{N_v}\right)^{-1} \beta D \tag{5.11}$$

It follows that,

$$\begin{aligned} \text{trace}\left(D^{-1/2} K_{\in} D^{-1/2}\right) &= K - \text{trace}\left(\beta D\beta^T \left(\beta D\beta^T + \sigma^2 I_{N_v}\right)^{-1}\right) \\ &= K - \sum_{i=1}^{N_v} \frac{\lambda_i}{\lambda_i + \sigma^2} \end{aligned} \tag{5.12}$$

where λ_i's are the eigenvalues of the matrix $\beta D\beta^T$. If the normalized MMSE for the user i is given by

$$\text{MMSE}_i = \frac{E(\hat{S}_i - S)}{p_i}$$

then the overall MMSE of the system becomes,

$$\text{MMSE} = \sum_{i=1}^{K} \text{MMSE}_i = K - \sum_{i=1}^{N_v} \frac{\lambda_i}{\lambda_i + \sigma^2} \tag{5.13}$$

The relationship between MMSE and SIR is well defined and can be easily verified

$$\text{MMSE}_i = \frac{1}{1 + SIR_i} \tag{5.14}$$

Therefore,

$$\sum_{i=1}^{K} \frac{SIR_i}{1+SIR_i} = K - \sum_{i=1}^{K} \mathrm{MMSE}_i$$

$$= \sum_{i=1}^{N_v} \frac{\lambda_i}{\lambda_i + \sigma^2} \tag{5.15}$$

Note that

$$tr(\Lambda) = tr\left(\beta D \beta^{\mathrm{T}}\right) \tag{5.16}$$

$$\left(\beta D \beta^{\mathrm{T}}\right)_{ij} = \beta_{il} d_{lk} \left(\beta^{T}\right)_{kj}$$

where Einstein summation[1] is used here to sum over repeated indices, it follows that

$$tr\left(\beta D \beta^{\mathrm{T}}\right) = \beta_{il} d_{lk} \left(\beta^{T}\right)_{ki}$$

Now using the property that $tr(AB) = tr(BA)$,

$$tr\left(\beta D \beta^{\mathrm{T}}\right) = \left(\beta^{T} \beta\right)_{kl} d_{lk}$$

Since β is the code vector matrix of l_2 norm 1,

$$tr\left(\beta D \beta^{\mathrm{T}}\right) = \delta_{kl} d_{lk} = d_{kk}$$

$$= tr(D) \tag{5.17}$$

---

[1] The convention that repeated indices are implicitly summed over. This can greatly simplify and shorten equations involving tensors. For example, using Einstein summation,

$$a_i a_i \equiv \sum_i a_i a_i$$

and

$$a_{ik} a_{ij} = \sum_i a_{ik} a_{ij}.$$

Now if $\overline{p} = \frac{1}{N_v}\sum_{i=1}^{K} p_i$, then the vector $\underbrace{(\overline{p}, \overline{p} \ldots, \overline{p})}_{N_v \text{ times}}$ is majorized by vector of eigenvalues $\left(\lambda_1, \lambda_2, \ldots, \lambda_{N_v}\right)$. At this point an important theorem in field of majorization is invoked which was proposed by Schur [25].

Theorem 5.1 A real valued function $\phi : R^n \rightarrow R$ is said to be Schur concave if for all $x, y \in R^n$, such that y majorizes x, then $\phi(x) \geq \phi(y)$. ϕ is Schur convex if $-\phi$ is Schur concave.

Theorem 5.2 If g: $\mathbb{R} \rightarrow \mathbb{R}$ is convex then the symmetric convex function,

$$\phi(x) = \sum_{i=1}^{n} g(x_i) \tag{5.18}$$

is Schur convex. By definition, g: $\mathbb{R} \rightarrow \mathbb{R}$ is concave then symmetric function,

$$\phi(x) = \sum_{i=1}^{n} g(x_i) \tag{5.19}$$

is Schur concave.

One can see easily that the map $x \rightarrow \frac{x}{x + \sigma^2}$ is concave in x and hence the symmetric concave map $\left(\lambda_1, \lambda_2, \ldots, \lambda_{N_v}\right) \rightarrow \sum_{i=1}^{N_v} \frac{\lambda_i}{\lambda_i + \sigma^2}$ is Schur concave. Then using Theorem 5.1 and Theorem 5.2 following is obtained,

$$\sum_{i=1}^{N_v} \frac{\lambda_i}{\lambda_i + \sigma^2} \leq \sum_{i=1}^{N_v} \frac{\overline{p}}{\overline{p} + \sigma^2} \tag{5.20}$$

Therefore from (5.15) and (5.20),

$$\sum_{i=1}^{K} \frac{SIR_i}{1+SIR_i} \leq \sum_{i=1}^{N_v} \frac{\overline{p}}{\overline{p}+\sigma^2} \tag{5.21}$$

Now for a given system, if the requirement of Signal to Interference Ratio (SIR) to be above a given threshold, i.e. $SIR_i \geq \mu$, then

$$K\frac{\mu}{1+\mu} \leq N_v \frac{\overline{p}}{\overline{p}+\sigma^2} \tag{5.22}$$

$$\overline{p} \geq \frac{K\mu\sigma^2}{N_v(1+\mu)-K\mu} \tag{5.23}$$

The expression (5.23) provides the number of users that can be admitted into a system with a given power and SIR. Lets now consider the two interference cases discussed in Section 5.1 and see their contribution to the above inequality.

Case 1: Constant Interference

For the constant interference, which is assumed to be known precisely at the central controller, the assumption of treating the interference as virtual additional users in the system was proposed. In such a case, $\overline{p}$ will be modified as $\overline{p} = \frac{1}{N_v}\sum_{i=1}^{K+1} p_i$, where, $p_1 = p_2 = \ldots = p_K = p$ are the powers associated with each user and p_{K+1} is the constant interference power. As a result,

$$\frac{Kp + p_{K+1}}{N_v} \geq \frac{(K+1)\mu\sigma^2}{N_v(1+\mu)-(K+1)\mu} \tag{5.24}$$

Above is a quadratic inequality in K which is the number of users admitted in the system. As can be easily seen for p_{K+1} =0, then it is the case when there is no interference, and the number of users that can be admitted are,

$$K \le N_v \left(1 + \frac{1}{\mu} - \frac{\sigma^2}{p}\right) \tag{5.25}$$

Case2: Narrowband Interference

For the narrowband interference which is not constant,

$$K \frac{\mu}{1+\mu} \le \sum_{i=1}^{N_v} \frac{\overline{p}}{\overline{p} + \sigma_N^2} \tag{5.26}$$

where σ_N^2 is no longer simply Gaussian noise at the receiver but also contains the narrowband noise which could be present in some or all of the frequency time slots. Therefore,

$$K \frac{\mu}{1+\mu} \le a\left(\frac{\overline{p}}{\overline{p} + \sigma^2}\right) + b\left(\frac{\overline{p}}{\overline{p} + \sigma^2 + \sigma_{NB}^2}\right) \tag{5.27}$$

where $a + b = N_v$, σ^2 is power of Gaussian noise, σ_{NB}^2 is narrowband interference power, present in b slots.

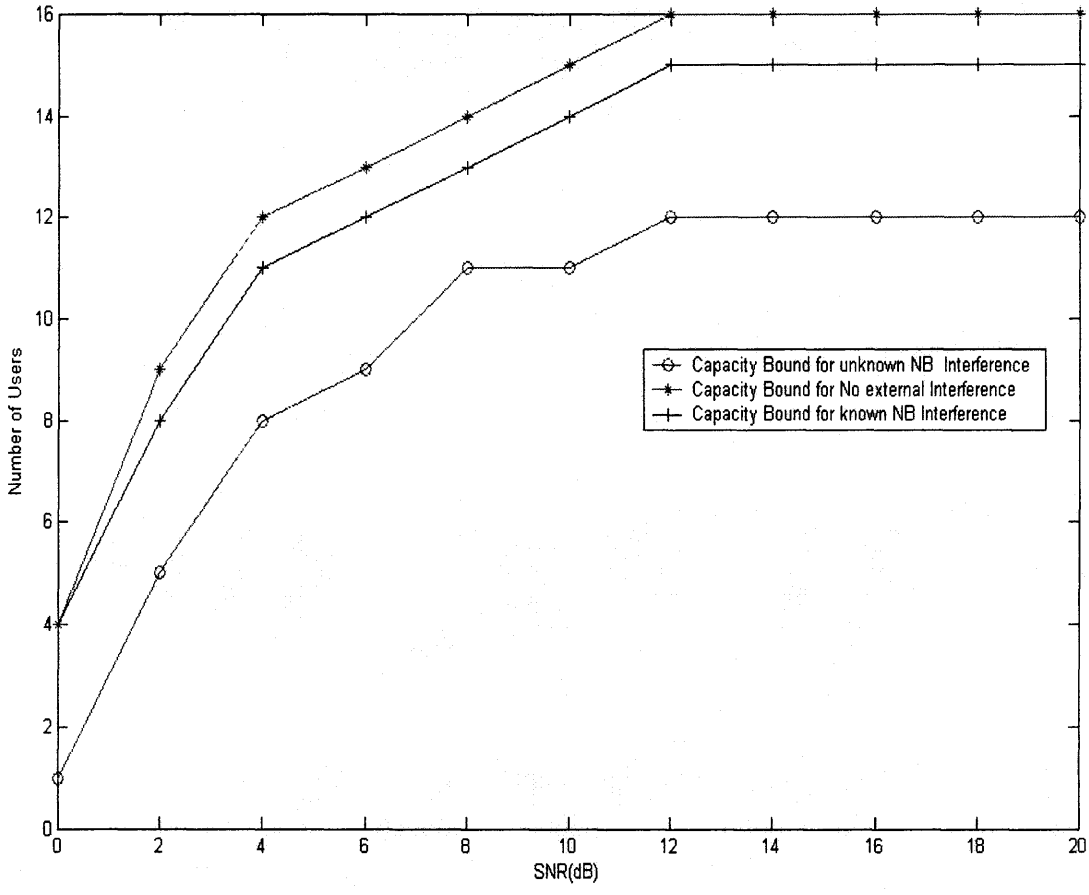

Figure 5.2 User capacity bound regions generated from equations (5.24), (5.25) and (5.27) for N_v=12, SIR= -5dB and system threshold i.e. μ=5dB. For equation (5.27), a=0 and b=12.

The Figures 5.3-5.10 show the error performance in presence of the two types of narrowband interferences discussed. The simulations were performed for K =10, 11 and 13 users with signature sequences of length N_v = 9 and for K=14 and 16 users with signature sequences of length N_v = 12. There were two cases considered, one in which the interference is present in all time-frequency slots (worst case scenario) and second in which the interference was present in only one of the frequency bands but at all times. It can be observed that the performance of the system in the cases considered, allows operation on the system in the particular band without significant deterioration. Therefore, if the coding

is combined with error correction techniques, the performance of the system can be boosted and unnecessary shutting off of the particular multiband in which NB interference exists can be avoided.

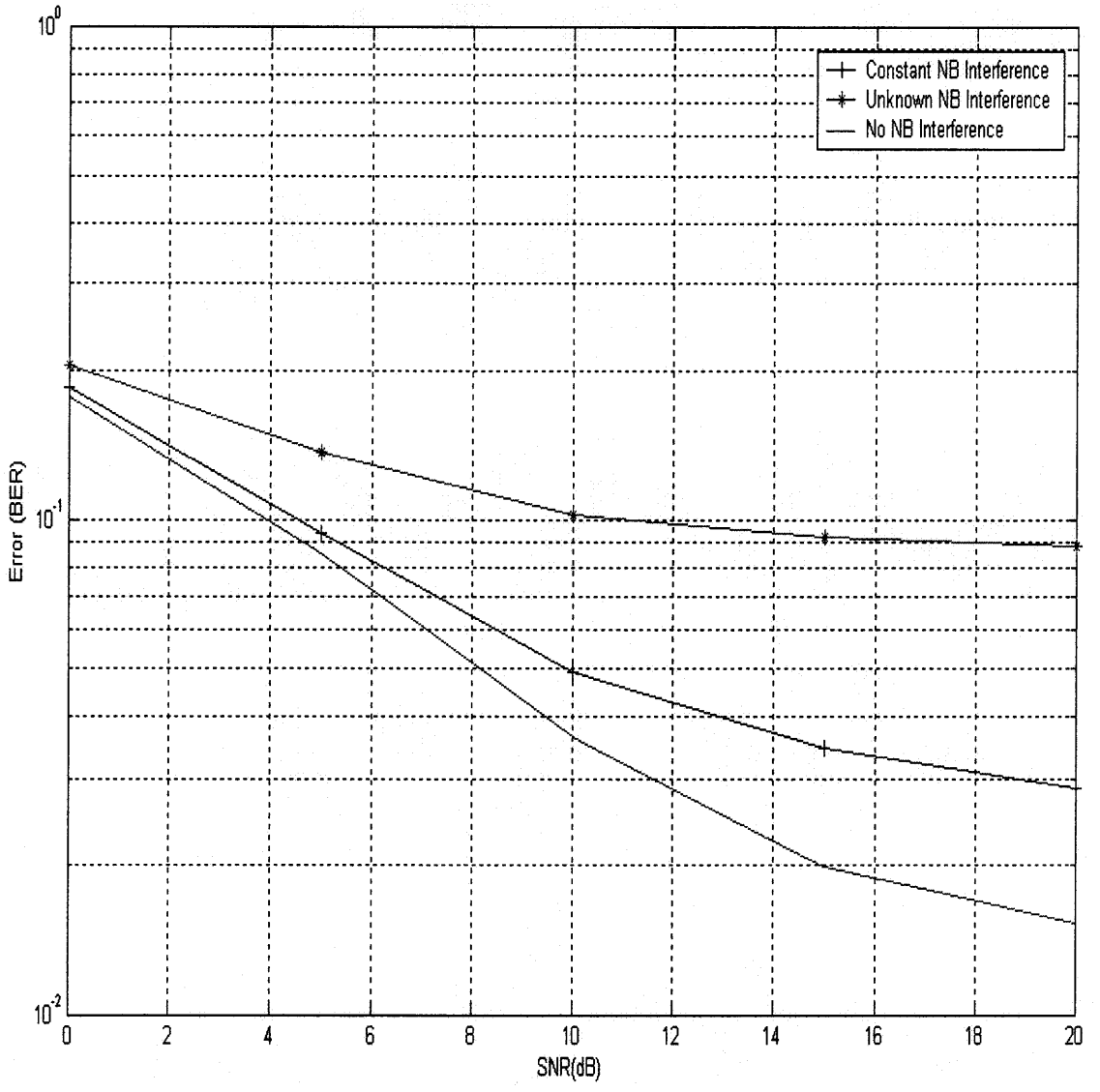

Figure 5.3 Error(BER) for the two different types of narrowband interferences when the interference exist in all the time frequency slots and Signal to Interference Ratio (SIR) is -10dB ($K = 11,\ N_v = 9$) .

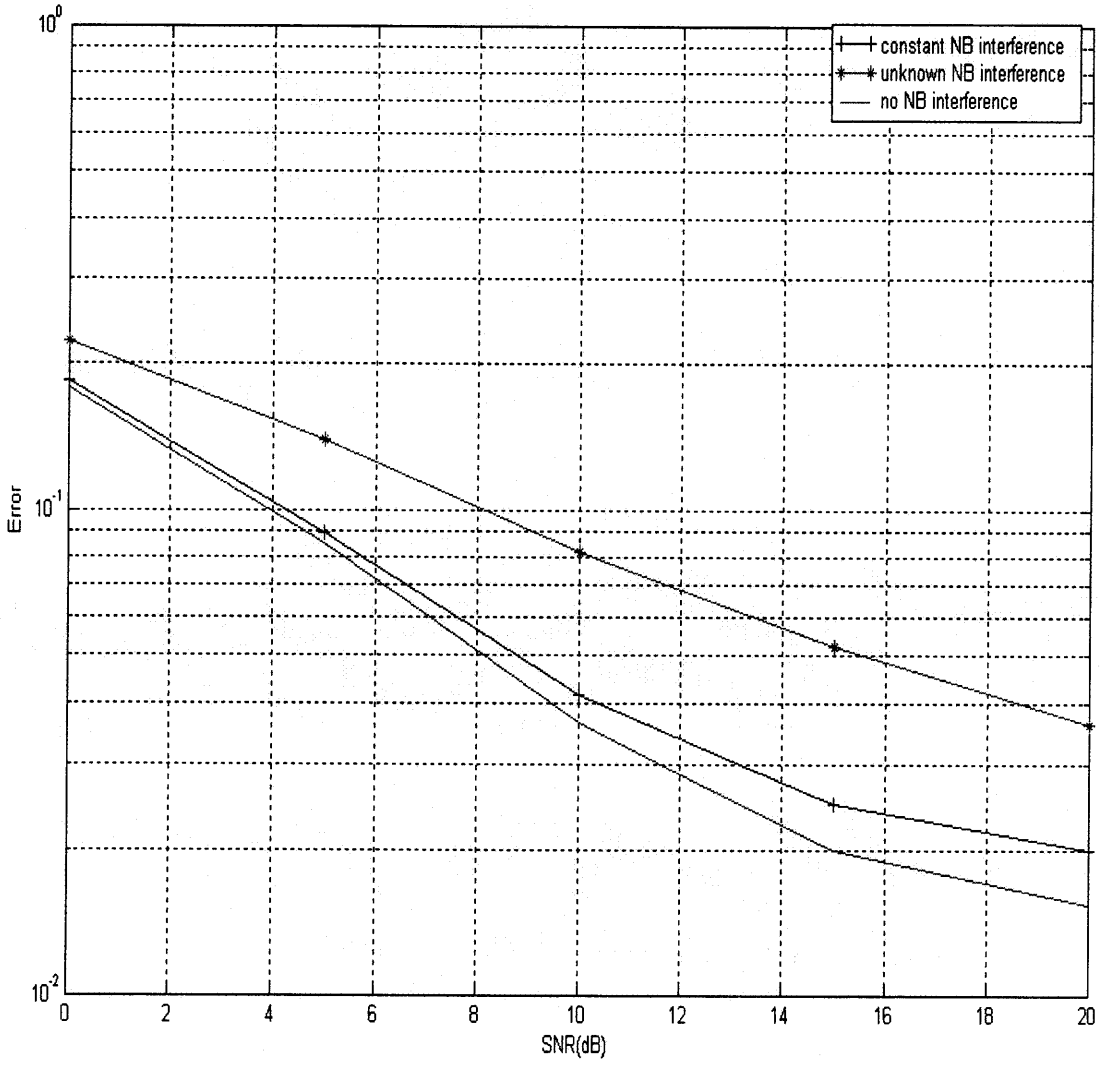

Figure 5.4 Error (BER) for the two different types of narrowband interferences when the interference exists in a single frequency band and along all time slots. Signal to Interference Ratio (SIR) is -10dB (K =11, N_v = 9).

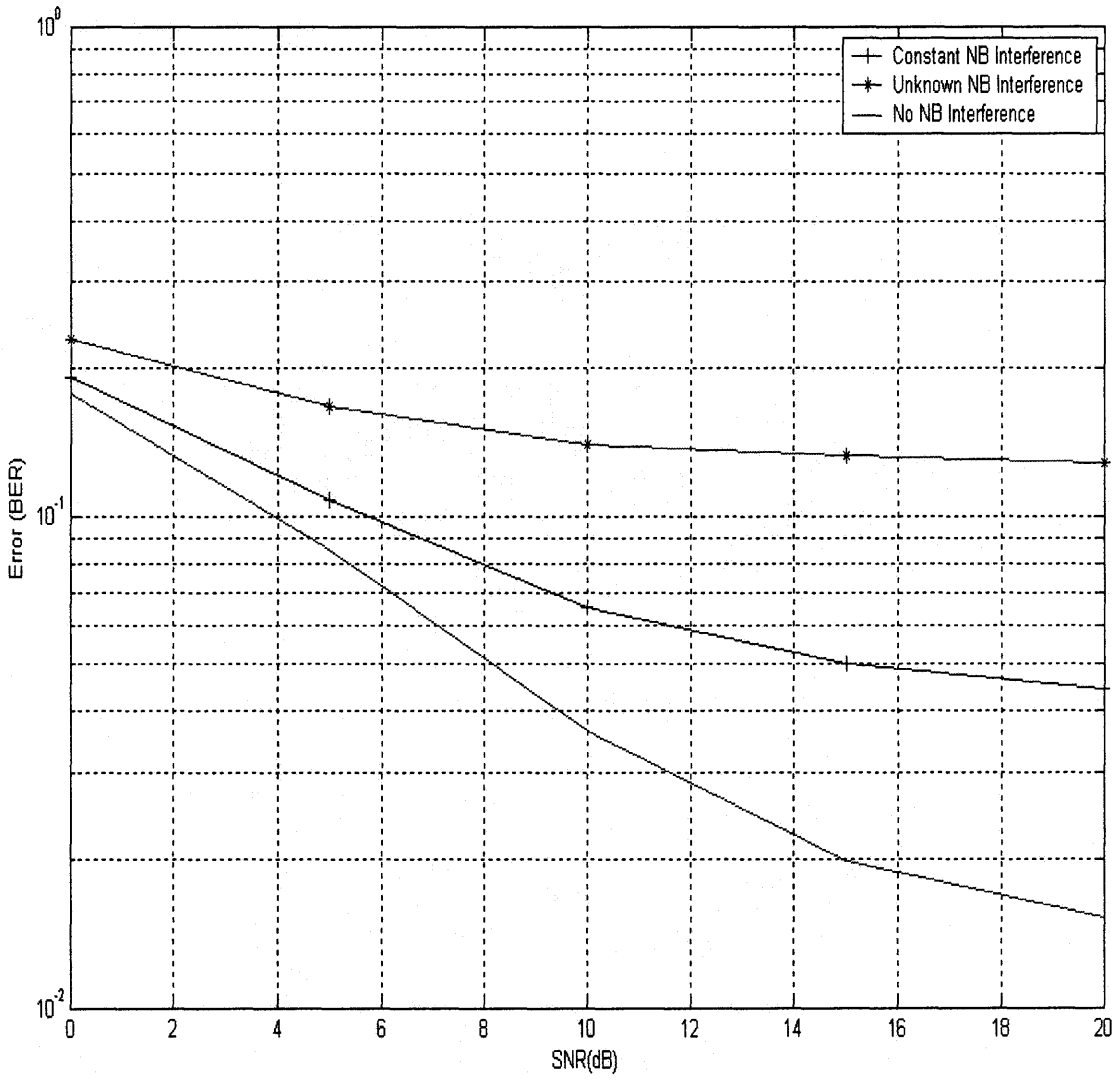

Figure 5.5 Error (BER) for the two different types of narrowband interferences when the interference exists in all the time frequency slots and Signal to Interference Ratio (SIR) is -5dB ($K = 11$, $N_v = 9$).

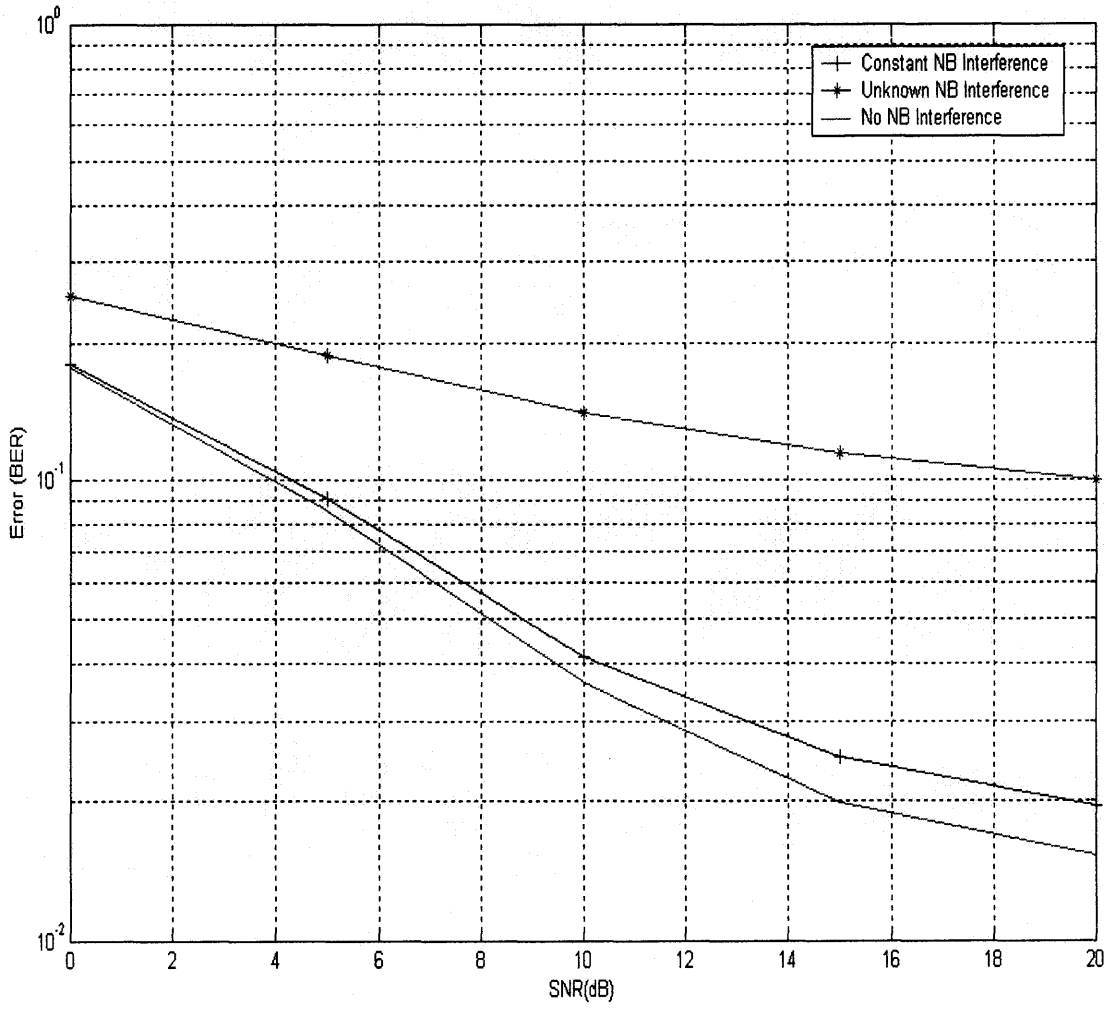

Figure 5.6 Error(BER) for the two different types of narrowband interferences when the interference exists in a single frequency band and along all time slots. Signal to Interference Ratio (SIR) is -5dB (K =11, N_v = 9).

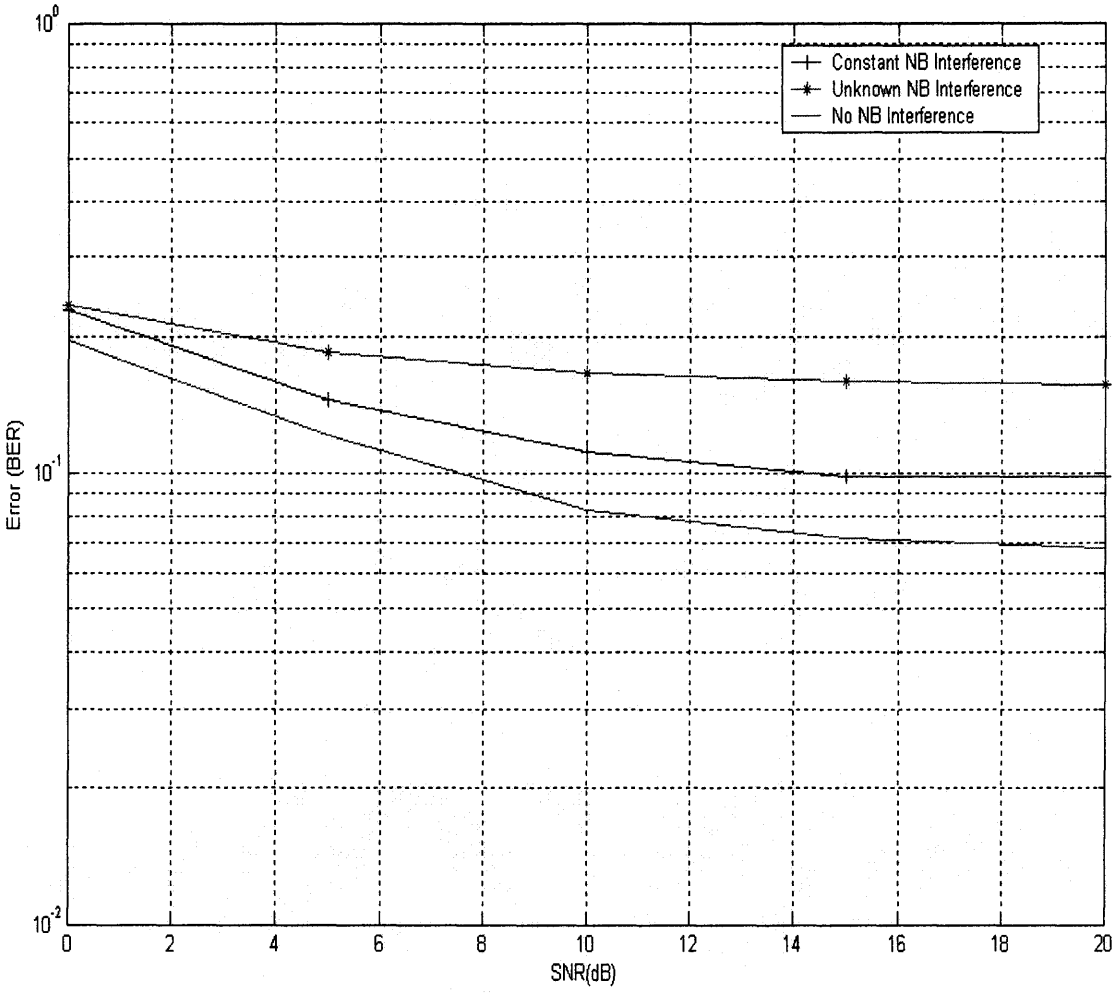

Figure 5.7 Error (BER) for the two different types of narrowband interferences when the interference exists in all the time frequency slots and Signal to Interference Ratio (SIR) is -5dB ($K = 13$, $N_v = 9$).

The above simulation result was generated for a system comprising of 13 users each having a code of length nine with interference assumed to be present in all frequency and time slots. It can be seen that despite presence of interference, the system can still be operated at a reduced capacity.

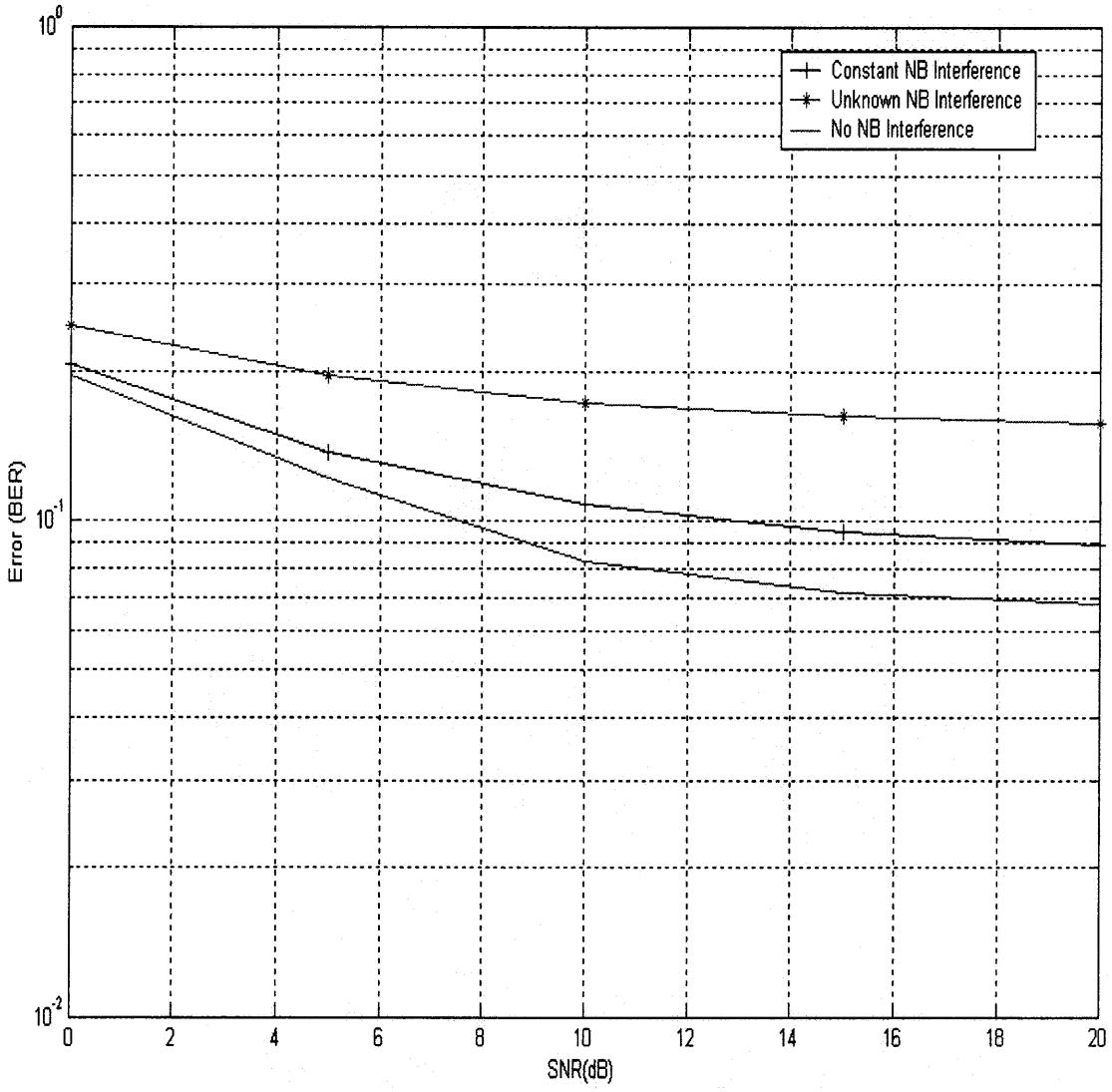

Figure 5.8 Error(BER) for the two different types of narrowband interferences when the interference exists in a single frequency band and along all time slots. Signal to Interference Ratio (SIR) is -5dB (K =13, N_v = 9).

CHAPTER 6

LANCZOS ALGORITHM FOR ITERATIVE CODE GENERATION

This chapter builds upon the iterative code generation discussed in Chapter 4 to efficiently implement it into the system under consideration. Lanczos algorithm is considered for increasing computational efficiency by simplifying the treatment of system of linear equations. The algorithm is employed in two different ways for minimizing the Mean Square Error of system in an iterative fashion to eventually achieve the final code set vector.

Evident from the proposed technique and mentioned before, large number of MMSE blocks are required. This can significantly increase computational requirements, primarily due to calculations involving inverse of large correlation matrix. In order to circumvent this, various techniques have been put forth, most important of which has been the Multi Stage Nested Weiner Filter [16] implementation, which significantly reduces the MMSE computations by obviating the need for calculating inverse of matrix through elegant iterative subspace decomposition technique. By employing reduced rank MSNWF filter there is a further reduction in computations and hence decrease in cost. Reduced rank of subspace for finding the solution to an MMSE problem has been of lot of interest in the field of filter theory. This has also motivated the primary objective of this chapter of using Lanczos algorithm to find a solution on Krylov subspace [ref for Krylov] of reduced rank.

6.1 Mean Square Error of the System

Recalling the Section 4.5, the Mean Square Error in the system can be expressed in terms of Total Squared Correlation. Assuming s_i , $i = 1,...,K$, are the signature sequences of the users. Again assuming like earlier, the transmitted power for all users to be same i.e. $p_i = p$ .If the received signal is **r** then the MSE for the i^{th} user is [12]

$$\begin{aligned} \mathrm{MSE_i} &= E\left[\left(\mathrm{r}^T s_i - b_i\right)^2\right] \\ &= s_i^T \left(p\sum_{j=1}^{K} s_j s_j^T + \sigma^2 \mathrm{I}_{\mathrm{N_v}} \right) s_i - 2\sqrt{p} s_i^T s_i + 1 \end{aligned}$$

The total MSE in the system will be

$$\begin{aligned} \mathrm{MSE} &= \sum_{i=1}^{K} \mathrm{MSE_i} \\ &= p\sum_{i=1}^{K}\sum_{j=1}^{K}\left(s_i^T s_j\right)^2 - \left(2\sqrt{p} - \sigma^2\right)\sum_{i=1}^{K} s_i^T s_i + K \end{aligned} \tag{6.1}$$

Observing that the first term in (6.1) is nothing but TSC and making use of the fact that the signature sequences are unit energy vectors

$$\mathrm{MSE} = p\mathrm{TSC} + \left(1 + \sigma^2 - 2\sqrt{p}\right)K \tag{6.2}$$

Equation (6.2) shows direct relationship between MSE and TSC. It therefore implies that MSE of the system can be decreased by correspondingly reducing the TSC.

$$\mathrm{TSC} = \left(s_k^T s_k\right)^2 + 2 s_k^T \left(\sum_{j \neq k} s_j s_j^T \right) s_k + \gamma_k \tag{6.3}$$

where

$$\gamma_k = \sum_{i \neq k} \sum_{j \neq k} \left(s_i^T s_j \right)^2 \tag{6.4}$$

Since all signature sequences are assumed to be unit energy vectors, (6.3) reduces to

$$\text{TSC} = 2 s_k^T A_k s_k + \gamma_k + 1 - 2\sigma^2 \tag{6.5}$$

where

$$A_k = \sum_{j \neq k} s_j s_j^T + \sigma^2 \mathrm{I}_{N_v} \tag{6.6}$$

Now, there are two ways of handling the issue of reducing the MMSE of the entire system. The approach can be, to either target the TSC directly or else the MMSE which is equivalent to solving the Wiener Hopf equation.

6.2 Eigendecomposition of TSC

The Total Squared Correlation (TSC) can be observed to be in a typical form such that if the signature waveform of the given user is the eigenvector corresponding to the minimum eigenvalue of the correlation matrix then the replacement of the old signature with the new eigenvector of the correlation matrix leads to decrease in TSC value for that particular iteration. This [13] is shown below.

$$\text{TSC} = 2 s_k^T A_k s_k + \gamma_k + 1 - 2\sigma^2$$

Taking the first expression on the right hand side of the above equation, and assuming that the k^{th} user replaces its current signature waveform with some vector z then the resulting difference in TSC is

$$\Gamma = tr\left((A_k + s_k s_k^T)^2 \right) - tr\left((A_k + z z^T)^2 \right) \tag{6.7}$$

where $tr(\bullet)$ represents the trace of the matrix.

After some algebraic manipulation it can be shown that $\Gamma \geq 0$ under the following condition

$$s_k^T A_k s_k + \|s_k\|_2^2 \geq z^T A_k z + \|z\|_2^2$$

This implies

$$s_k^T A_k s_k \geq z^T A_k z \tag{6.8}$$

if $\|s_k\|_2^2 = \|z\|_2^2$ which is what will be assumed henceforth. Now if the chosen vector replacement of the present signature is chosen as the eigenvector of the correlation matrix then according to the Rayleigh quotient theorem, if $z = q_i$

$$\lambda_i = \frac{q_i^T A_k q_i}{q_i^T q_i} \tag{6.9}$$

where q_i is the eigenvector corresponding to the i^{th} eigenvalue λ_i. If $q_i^T q_i = 1$ then

$$\lambda_i = q_i^T A_k q_i \tag{6.10}$$

Now if the eigenvalue is the minimum eigenvalue of the correlation matrix then the replacing signature waveform with eigenvector η, corresponding to this minimum eigenvalue would result in largest reduction in TSC or in other words the least TSC.

$$\lambda_{\min} = \eta^T A_k \eta = \min_{s_k} TSC \tag{6.11}$$

Therefore, replacing the signature waveform with the eigenvector of the correlation matrix corresponding to the minimum eigenvalue would appear as the best solution to the problem at hand. However the eigendecomposition of the entire matrix followed by search for the minimum eigenvalue can be computational intensive.

Therefore, an algorithm needs to be developed that reduces this search for the minimum eigenvalue over the entire subspace spanned by the eigenvectors of the matrix to a reduced subspace. At the same time the estimation of the minimum eigenvalue has to be good enough to avoid serious errors.

6.3 Lanczos Algorithm

Lanczos algorithm is an efficient way of handling the problem of reduced subspace search for the extremal eigenvalues of the correlation matrix. The method involves partial tridiagonalizations of the given matrix. Information about the given matrix's extremal eigenvalues tends to emerge long before tridiagonalization is complete which describes its usefulness when only the largest or smallest eigenvalues are desired. Tridiagonalization by itself also provides and effective way of solving linear equations, a property which shall be exploited later.

It is preferred to lead into discussion of derivation of Lanczos algorithm by considering the optimization of Rayleigh quotient

$$r(y) = \frac{y^T A_k y}{y^T y} \qquad y \neq 0 \tag{6.12}$$

Replacing the correlation matrix A_k in the above expression by a matrix A in general. From the minimax theorem it is known that the minimum and maximum values of $r(y)$ are minimum eigenvalue $\lambda_{\min}$, and maximum eigenvalue $\lambda_{\max}$ of the matrix

respectively. Suppose $\{u_i\} \subseteq \mathbb{R}^n$ is a sequence of orthonormal vectors and define the scalars

$$M_k = \lambda_{\max}\left(U_k^T A U_k\right) = \max_{y\neq 0} \frac{y^T\left(U_k^T A U_k\right)y}{y^T y} = \max_{y\neq 0} r(U_k y) \leq \lambda_{\max}(A)$$

$$m_k = \lambda_{\min}\left(U_k^T A U_k\right) = \min_{y\neq 0} \frac{y^T\left(U_k^T A U_k\right)y}{y^T y} = \min_{y\neq 0} r(U_k y) \geq \lambda_{\min}(A) \tag{6.12}$$

where $U_k = [u_1, ..., u_k]$. The Lanczos algorithm can be derived by considering how to generate the u_k so that M_k and m_k are increasingly better estimates of $\lambda_{\max}$ and $\lambda_{\min}$. Both the above requirements can be satisfied simultaneously by the same U_k which are the basis function of the Krylov subspace, as shown in [27].

$$\mathcal{K}(A, u_1, k) = span\left\{u_1, Au_1, ..., A^{k-1}u_1\right\} \tag{6.13}$$

which is the range space of

$$K(A, u_1, k) = \left[u_1, Au_i, ...A^{k-1}u_1\right] \tag{6.14}$$

6.3.1 Tridiagonalization

In order to find this basis efficiently, one can exploit the connection between the tridiagonalization of A and QR factorization of $K(A, u_1, k)$.

Theorem 6.1: If $U^T A U = T$ is tridiagonal decomposition of the symmetric matrix $A \in \mathbb{R}^{n\times n}$, then $U^T K(A, U(:,1), n) = R$ is upper triangular.

Proof. It is clear that $u_1 = U(:,1)$, then

$$U^T K(A,U(:,1),k) = \left[U^T u_1, (U^T AU)U^T u_1, ...(U^T AU)^{n-1} U^T u_1\right]$$
$$= \left[e_1, Te_1, ..., T^{n-1} e_1\right] = R \tag{6.15}$$

is upper triangular with property that $r_{11} = 1$ and $r_{ii} = t_{21} t_{32} ... t_{i,i-1}$ for $i = 2:n$.

Tridiagonalization can be performed using sequence of Householder transformation, but if the given correlation matrix is large and sparse then, then the mentioned technique tends to destroy sparsity. Therefore, one can resort to directly computing the elements of tridiagonal matrix $T = U^T AU$. Setting $U = [u_1, ..., u_n]$

$$T = \begin{bmatrix} \alpha_1 & \beta_1 & \cdots & 0 \\ \beta_1 & \alpha_2 & \ddots & \vdots \\ & \ddots & \ddots & \ddots \\ \vdots & & \ddots & \ddots & \beta_{n-1} \\ 0 & \cdots & & \beta_{n-1} & \alpha_n \end{bmatrix} \tag{6.16}$$

and equating columns in $AU = UT$, it is observed

$$Au_k = \beta_{k-1} u_{k-1} + \alpha_k u_k + \beta_k u_{k+1} \tag{6.17}$$

for k = 1:n-1. The orthonormality of the u_i implies $\alpha_k = u_k^T A_k u_k$. Moreover, if $r_k = (A - \alpha_k I)u_k - \beta_{k-1} u_{k-1}$ is non-zero, then $u_{k+1} = r_k / \beta_k$ and $\beta_k = \|r_k\|_2$. If $r_k = 0$, then the iteration breaks down but not without acquisition of valuable invariant subspace information. Therefore, by properly sequencing the above formulae one obtains the Lanczos algorithm.

Lanczos Algorithm

$r_0 = u_1$
$\beta_0 = 1$
$u_0 = 0$
$k = 0$
$while(\beta_k \neq 0)$
$u_{k+1} = r_k / \beta_k$
$k = k + 1$
$\alpha_k = u_k^T A_k u_k$
$r_k = (A - \alpha_k I)u_k - \beta_{k-1} u_{k-1}$
$\beta_k = \|r_k\|_2$
end

Theorem 6.2: Let $A \in \mathbb{R}^{n\times n}$ be symmetric and assume $u_1 \in \mathbb{R}^n$ has unit 2-norm. Then Lanczos iteration runs until $k = m$, where $m = rank(K(A,u_1,n))$. Moreover, for $k = 1:m$

$$AU_k = U_k T_k + r_k e_k^T \tag{6.18}$$

where

$$T_k = \begin{bmatrix} \alpha_1 & \beta_1 & \cdots & 0 \\ \beta_1 & \alpha_2 & \ddots & \vdots \\ & \ddots & \ddots & \ddots \\ \vdots & & \ddots & \beta_{k-1} \\ 0 & \cdots & \beta_{k-1} & \alpha_k \end{bmatrix} \tag{6.19}$$

and $U_k = [u_1,....,u_k]$ has orthonormal columns that span $\mathcal{K}(A,u_1,k)$.

Proof. The proof is by induction on k. Suppose the iteration has produced $U_k = [u_1,....,u_k]$ such that $range(U_k) = \mathcal{K}(A,u_1,k)$ and $U_k^T U_k = I_k$. It is easy to see

from equation (6.17) that expression (6.18) holds. Thus, $U_k^T A U_k = T_k + U_k^T r_k e_k^T$. Since $\alpha_i = u_i^T A u_i$ for i =*1: k* and

$$u_{i+1}^T A u_i = u_{i+1}^T \left(A u_i - \alpha_i u_i - \beta_{i-1} u_{i-1} \right) = u_{i+1}^T \beta_i u_{i+1} = \beta_i \tag{6.20}$$

for i = *1: k-1*, $U_k^T A U_k = T_k$. Consequently, $U_k^T r_k = 0$.

If $r_k \neq 0$, then $u_{k+1} = r_k / \|r_k\|_2$ is orthogonal to $u_1, \ldots, u_k$ and

$$u_{k+1} \in span\{A u_k, u_k . u_{k-1}\} \subseteq \mathcal{K}(A, u_1, k+1) \tag{6.21}$$

Thus, $U_{k+1}^T U_{k+1} = I_{k+1}$ and $range(U_{k+1}) = \mathcal{K}(A, u_1, k+1)$. On the other hand, if $r_k = 0$, then $A U_k = U_k T_k$. This says that $range(U_k) = \mathcal{K}(A, u_1, k)$ is invariant. From this one concludes that $k = m = rank(K(A, u_1, n))$.

Encountering a zero β_k is a welcome event in that it signals the computation of an exact invariant subspace. However, an exact zero or even a small β_k is a rarity in practice. The following theorems provide insight into the property of Lanczos algorithm and its convergence for reduced eigenspace search for extremal eigenvalues.

Theorem 6.3: Suppose that k steps of Lanczos algorithm have been performed and that $S_k^T T_k S_k = diag(\theta_1, \ldots, \theta_k)$ is the Schur decomposition of the tridiagonal matrix T_k. If $Y_k = [y_1, \ldots, y_k] = U_k S_k \in \mathbb{R}^{n \times k}$, then for i =*1: k*, $\|A y_i - \theta_i y_i\|_2 = |\beta_k| |s_{ki}|$ where

Proof. Post multiplying equation (6.18) by S_k gives

$$A Y_k = Y_k diag(\theta_1, \ldots, \theta_k) + r_k e_k^T S_k \tag{6.22}$$

and so $Ay_i = \theta_i y_i + r_k\left(e_k^T S_k e_i\right)$. The proof is complete by taking the norms and recalling $\|r_k\|_2 = |\beta_k|$.

The theorem provides computable error bounds for T_k's eigenvalues.

$$\min_{\tau \in \lambda(A)} |\theta_i - \tau| \le |\beta_k||s_{ki}| \qquad \text{for } i = 1{:}\ k \tag{6.23}$$

At this point, there lies an interest in knowing the rate of convergence of eigenvalues of T_k to those of the matrix A. The following theorem gives details of the convergence rate of the eigenvalues via Lanczos algorithm.

Theorem 6.4: Let A be an n-by-n symmetric matrix with eigenvalues $\lambda_1 \ge \lambda_2 \ge \cdots \ge \lambda_n$ and corresponding orthonormal eigenvectors $z_1, \ldots, z_n$. If $\theta_1 \ge \theta_2 \ge \cdots \ge \theta_k$ are the eigenvalues of the matrix T_k obtained after k of the Lanczos iteration, then

$$\lambda_1 \ge \theta_1 \ge \lambda_1 - \frac{(\lambda_1 - \lambda_n)\tan(\phi_1)^2}{\left(c_{k-1}(1+2\rho_1)\right)^2} \tag{6.24}$$

where $\cos(\phi_1) = |u_1^T z_1|$, $\rho_1 = (\lambda_1 - \lambda_2)/(\lambda_2 - \lambda_n)$, and $c_{k-1}(x)$ is the Chebyshev polynomial of degree $k-1$.

$$\lambda_n \le \theta_k \le \lambda_n + \frac{(\lambda_1 - \lambda_n)\tan(\phi_n)^2}{\left(c_{k-1}(1+2\rho_n)\right)^2} \tag{6.25}$$

where $\rho_n = (\lambda_{n-1} - \lambda_n)/(\lambda_1 - \lambda_{n-1})$ and $\cos(\phi_n) = |u_n^T z_n|$.

Proof. The proof is omitted here but interested readers can refer to [28] for detailed proof of above.

Theorems 6.3 and 6.4 provide valuable insights into convergence and convergence rates of the eigenvalues of matrix T_k to those of A. The Chebyshev polynomials that are found in denominator of the expressions (6.24) and (6.25) are bounded by unity on [-1, 1], but grow very rapidly outside this interval. Therefore the convergence rates of this technique involving the tridiagonalization through Lanczos method are very fast providing us with efficient solution to the parent problem by effectively reducing the dimensions of the subspace search. Figure 6.1 and Figure 6.2 shows the performance of the Multiband OFDM system when codes are generated using Lanczos algorithm, that determines the Ritz pair, comprising the eigenvector and associated minimum eigenvalue of the tridiagonal matrix T_k closest to the minimum eigenvalue of the correlation matrix A_k.

However, another approach to solving the search for the optimum code set could be the one discussed in Chapter 4 which was put forth in [12]. The solution involves minimization of error of each user in the system until the overall MMSE of the system is minimized and convergence is achieved resulting in optimal code set. This minimization which is in effect solving Weiner Hopf equations is a unique minimizer of the cost function [17] shown below. It is known that the error J produced by a transversal filter [eq.(5.50), 17] is given by

$$J = \sigma_{b_i}^2 - s^T r_{y,b_i} - r_{y,b_i}^T s + s^T R_y s \tag{6.26}$$

where $\sigma_{b_i}^2$ is the energy of the i^{th} users power, r_{y,b_i} is the cross correlation between the received signal and the i^{th} user's data bit and R_y is the correlation matrix of the received

signal y. From equation (6.26) it can be seen that the filter function that minimizes the error function would minimize the following cost function

$$\psi(s) = \frac{1}{2}\left(s^T R_y s\right) - s^T r_{y,b_i}$$

$$= \frac{1}{2}\left(s^T A_i s\right) - s^T s_i \tag{6.27}$$

The unique solution to the above is contained in putting its gradient equal to zero. This results in finding the solution to the following linear equation.

$$A_i s = s_i \tag{6.28}$$

It follows from expression (6.27),

$$s = A_i^{-1} s_i \tag{6.29}$$

When the current code vector of a particular user is replaced with normalized MMSE filter vector, then one obtains the iterative algorithm as proposed by [12]. However, in order to reduce complexity of computing the inverse of the given correlation, an approximate solution is derived. One such approximate solution can be arrived upon by MSNWF implementation of MMSE [16]. However, MSNWF requires computing the blocking matrix while implementation of MSNWF using Arnoldi algorithm provides a complex architecture of iterative pre-filter coefficients. Here Lanczos algorithm will be considered for simplification.

Suppose $s^{(0)} \in \mathbb{R}^n$ is the initial guess. One way to produce a vector sequence $\{s^{(k)}\}$ that converges to s is to generate a sequence of orthonormal vectors $\{u_k\}$ which are the basis of the Krylov subspace and let $s^{(k)}$ minimize ψ over the set

$$s^{(0)} + span\{u_1, \ldots, u_k\} = s^{(0)} + span\{u_1, A_i u_1 \ldots, A_i^{k-1} u_1\}$$

for $k=1: n$. If $U_k = [u_1, \ldots, u_k]$, then this just means choosing $\omega \in \mathbb{R}^k$ such that

$$\psi(s^{(0)} + U_k\omega) = \frac{1}{2}\left(s^{(0)} + U_k\omega\right)^T A_i\left(s^{(0)} + U_k\omega\right) - \left(s^{(0)} + U_k\omega\right)^T s_i$$

$$= \frac{1}{2}\omega^T\left(U_k^T A_i U_k\right)\omega - \omega^T U_k^T\left(s_i - A_i s^{(0)}\right) + \psi\left(s^{(0)}\right) \qquad (6.30)$$

is minimized. By taking the gradient of the (6.30) w.r.t ω one obtains

$$s^{(k)} = s^{(0)} + U_k\omega_k \qquad (6.31)$$

where

$$\left(U_k^T A_i U_k\right)\omega_k = U_k^T\left(s_i - A_i s^{(0)}\right) \qquad (6.32)$$

When $k = n$ the minimization is over all of $\mathbb{R}^n$ and so $A_i s^{(n)} = s_i$.

For large sparse A_i it is necessary to overcome two hurdles in order to make this effective solution process:

- The linear system (6.32) must be easily solved
- $s^{(k)}$ must be computed without having to refer to $u_1, \ldots, u_k$ explicitly as (6.31) suggests. Otherwise there would be an excessive amount of data movement.

It can be seen that both these requirements are met if u_k are Lanczos vectors.

After k steps of Lanczos algorithm one obtains the factorization

$$AU_k = U_k T_k + r_k e_k^T \qquad (6.33)$$

where

$$T_k = U_k^T A_i U_k = \begin{bmatrix} \alpha_1 & \beta_1 & \cdots & 0 \\ \beta_1 & \alpha_2 & \ddots & \vdots \\ & \ddots & \ddots & \ddots \\ \vdots & & \ddots & \ddots & \beta_{k-1} \\ 0 & \cdots & & \beta_{k-1} & \alpha_k \end{bmatrix} \qquad (6.34)$$

With this approach (6.32) becomes a symmetric positive definite tridiagonal system which may be solved via the LDL^T factorization. In particular, by setting

$$L_k = \begin{bmatrix} 1 & 0 & \cdots & 0 \\ \mu_1 & 1 & \ddots & \vdots \\ & \ddots & \ddots & \ddots \\ \vdots & & \ddots & \ddots & 0 \\ 0 & \cdots & & \mu_{k-1} & 1 \end{bmatrix} \quad \text{and} \quad D_k = \begin{bmatrix} d_1 & 0 & \cdots & 0 \\ 0 & d_2 & \ddots & \vdots \\ & \ddots & \ddots & \ddots \\ \vdots & & \ddots & \ddots & 0 \\ 0 & \cdots & 0 & d_k \end{bmatrix} \tag{6.35}$$

it is found by comparing entries in

$$T_k = L_k D_k L_k^T \tag{6.36}$$

that

$$\begin{aligned} &for\ i = 1:k \\ &\quad \mu_{i-1} = \beta_{i-1}/d_{i-1} \\ &\quad d_i = \alpha_i - \beta_{i-1}\mu_{i-1} \\ &end \end{aligned} \tag{6.37}$$

In order to obtain L_{k-1} and D_{k-1} from L_k and D_k one needs to calculate only the quantities

$$\begin{aligned} \mu_{k-1} &= \beta_{k-1}/d_{k-1} \\ d_k &= \alpha_k - \beta_{k-1}\mu_{k-1} \end{aligned} \tag{6.38}$$

In order to compute $s^{(k)}$ efficiently, let us define $C_k \in \mathbb{R}^{n\times k}$ and $z_k \in \mathbb{R}^k$ by the equation

$$C_k L_k^T = U_k \tag{6.39}$$

$$L_k D_k z_k = U_k^T \left(s_i - A_i s^{(0)}\right) \tag{6.40}$$

and observe that

$$s^{(k)} = s^{(0)} + U_k T_k^{-1} U_k^T s_i = s^{(0)} + U_k \left(L_k D_k L_k^T \right)^{-1} U_k^T s_i$$

$$= s^{(0)} + C_k z_k \tag{6.41}$$

Let $C_k = [c_1, \ldots, c_k]$ be a column partitioning. It follows from equation (6.39) that

$$[c_1, \mu_1 c_1 + c_2, \ldots, \mu_{k-1} c_{k-1} + c_k] = [u_1, \ldots, u_k] \tag{6.42}$$

and therefore $C_k = \left[C_{k-1}, c_k \right]$ where

$$c_k = u_k - \mu_{k-1} c_{k-1} \tag{6.43}$$

Also observe that if one sets $z_k = \left[\rho_1, \ldots, \rho_k \right]^T$ in $L_k D_k z_k = U_k^T s_i$, then that equation becomes {partitioned matrix expression)

Since $L_{k-1} D_{k-1} z_{k-1} = U_{k-1}^T s_i$, it follows that

$$z_k = \begin{bmatrix} z_{k-1} \\ \rho_k \end{bmatrix} \tag{6.44}$$

where

$$\rho_k = \left(u_k^T s_i - \mu_{k-1} d_{k-1} \rho_{k-1} \right) / d_k \tag{6.45}$$

and thus,

$$s^{(k)} = s^{(0)} + C_k z_k = s^{(0)} + C_{k-1} z_{k-1} + \rho_k c_k \tag{6.46}$$

From the first condition stated earlier for the desired algorithm, this is the precisely the recursive relation for x_k that is needed. Together with (6.38), (6.39) and (6.40) it enables us to make the transition from $(u_{k-1}, c_{k-1}, x_{k-1})$ to (u_k, c_k, x_k) with minimal work and storage.

A further simplification results if one sets u_1 to be unit vector in the direction of the initial residual $\left(s_i - A_i s^{(0)} \right)$. With this choice Lanczos starting vector,

$u_i^T\left(s_i - A_i s^{(0)}\right) = 0$ *for* $i \geq 0$. It follows from (6.33) that,

$$s_i - A_i x_k = s_i - A_i\left(s^{(0)} + U_k \omega_k\right) = \left(s_i - A_i s^{(0)}\right) - \left(U_k T_k + r_k e_k^T\right)\omega_k$$
$$= \left(s_i - A_i s^{(0)}\right) - U_k U_k^T\left(s_i - A_i s^{(0)}\right) - r_k e_k^T \omega_k = -r_k e_k^T \omega_k$$

(6.47)

Thus, if $\beta_k = \|r_k\|_2 = 0$ in the Lanczos iteration, then $A_i s^{(k)} = s_i$. Moreover, $\left\|A_i s^{(k)} - s_i\right\|_2 = \beta_k \left|e_k^T \omega_k\right|$ and so estimates of current residual can be obtained as a by product of the iteration. Overall, the procedure is as given below:

Algorithm

$r^{(0)} = s_i - A_i s^{(0)}$

$\beta_0 = \left\|r^{(0)}\right\|_2$

$u_0 = 0$

$k = 0$

while $\beta_k \neq 0$

$u_{k+1} = r^{(k)} / \beta_k$

$k = k + 1$

$\alpha_k = u_k^T A_i u_k$

$r_k = (A_i - \alpha_k I)u_k - \beta_{k-1} u_{k-1}$

$\beta_k = \|r_k\|_2$

if $k = 1$

$d_1 = \alpha_1$

$c_1 = u_1$

$\rho_1 = \beta_0 / \alpha_1$

$s^{(1)} = \rho_1 u_1$

Algorithm
(Contd.)

else

$$\mu_{k-1} = \beta_{k-1} / d_{k-1}$$
$$d_k = \alpha_k - \beta_{k-1}\mu_{k-1}$$

if $k = 1$

$$d_1 = \alpha_1$$
$$c_1 = u_1$$
$$\rho_1 = \beta_0 / \alpha_1$$
$$s^{(1)} = \rho_1 u_1$$

else

$$\mu_{k-1} = \beta_{k-1} / d_{k-1}$$
$$d_k = \alpha_k - \beta_{k-1}\mu_{k-1}$$
$$c_k = u_k - \mu_{k-1}c_{k-1}$$
$$\rho_k = -\ \mu_{k-1}d_{k-1}\rho_{k-1} / d_k$$
$$s^{(k)} = s^{(k-1)} + \rho_k c_k$$

end

end

$$\hat{s}_i = s^{(k)}$$

Therefore, either of the above discussed approaches can be used to compute the final set of codes for all users present in the system in an effective and efficient manner. Figure 6.1 and Figure 6.2 show the comparison in convergence of TSC for different techniques. The reduced space eigendecomposition converges faster than MMSE algorithm. This is understandable for the eigendecomposition algorithm gives the least TSC at each iteration. Figure 6.2 which shows considers reduced rank eigenspace

algorithm of rank two, three and four, shows nearly same performance for rank three and rank four suggesting that order three tridiagonal matrix would be sufficient for computing the eigenvector corresponding to the least eigenvalue thereby decreasing computational requirement.

Hence, the technique proposed in Chapter 4, in conjunction with employing the methods discussed in this chapter for efficiently computing the set of code vectors for different users, would help establish a short range wireless network in future on a Multiband OFDM backbone. Such a network would be able to support large number of wireless devices and should continue to deliver high speed performance. Even though such a system may modify peer to peer communications into one with all communications through central controller, the system can revert to peer to peer communications if the number of active devices in the system, are very few.

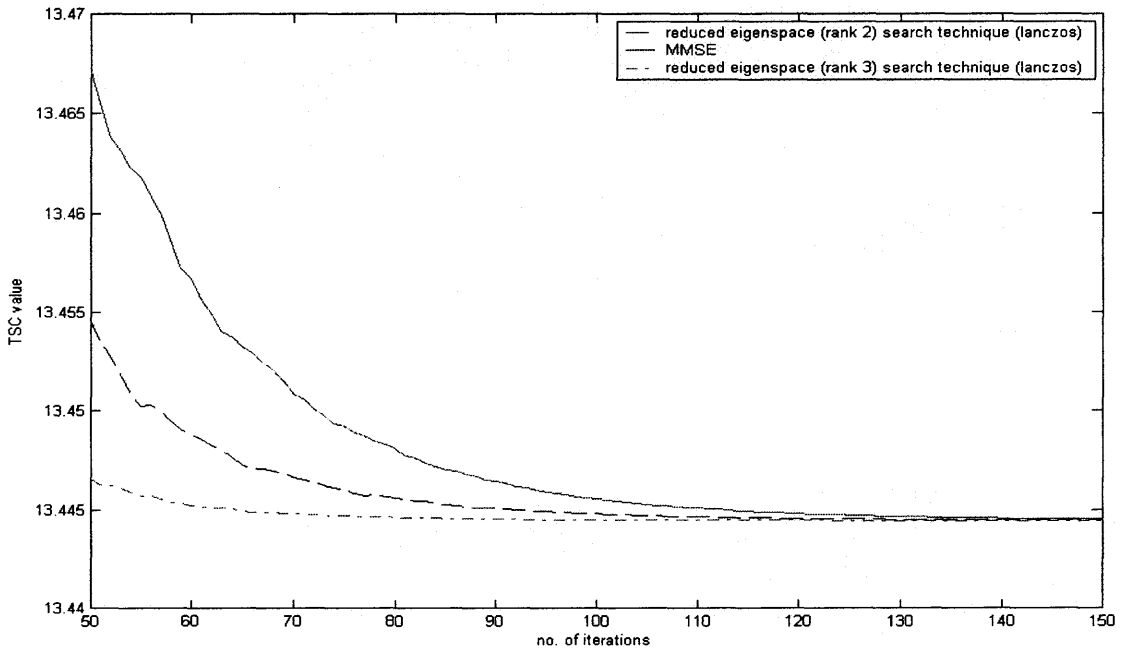

Figure 6.1 Convergence comparison for reduced rank eigenspace Lanczos algorithm and MMSE replacement algorithm for K=11 users with code of length N_v = 9 and SNR =10dB. Reduced rank eigenspace algorithm converges faster.

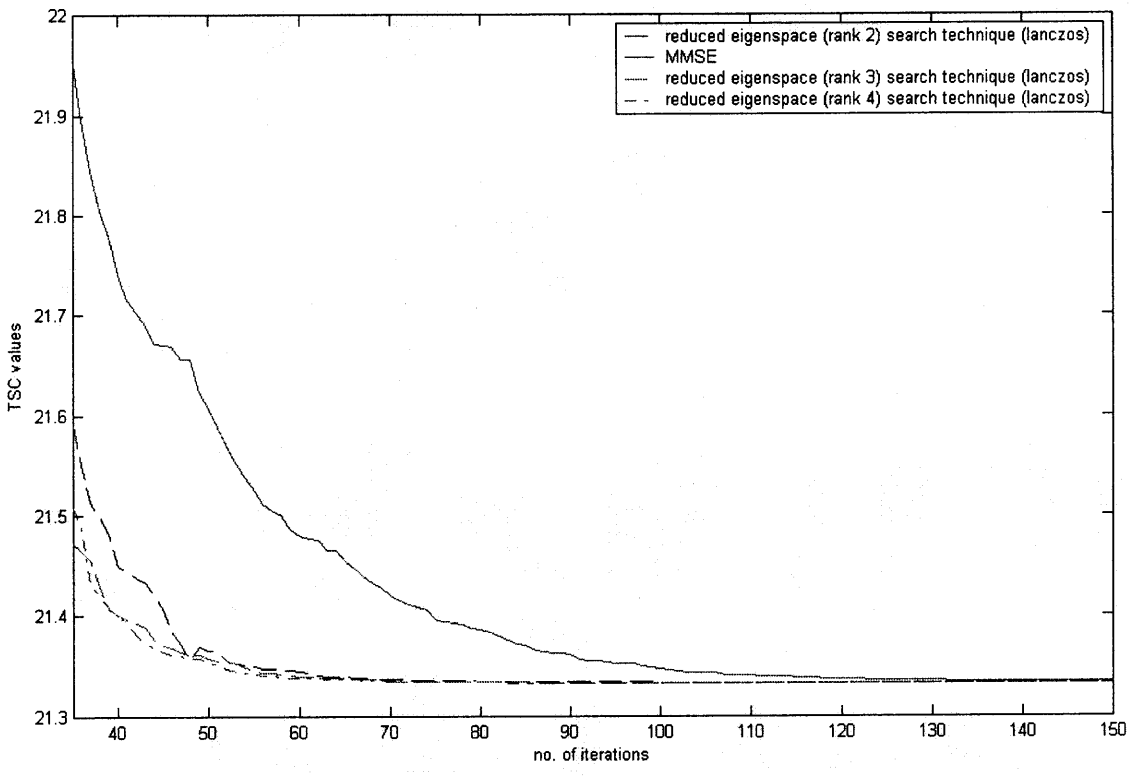

Figure 6.2 Convergence comparison for reduced rank eigenspace Lanczos algorithm and MMSE replacement algorithm for K=16 users with code of length $N_v = 12$ and SNR =10dB. Reduced rank eigenspace algorithm converges faster.

6.4 Conclusion

In this chapter, efficient implementation for iterative code generation algorithm was observed. While one implementation led to a fast convergence, the other provided effective implementation of MMSE filter without the need for correlation matrix inversion. Thus, using either algorithm for the proposed system in Chapter 4 will optimize the system in efficiency and design simplification.

REFERENCES

1. M. Z. Win and R. A. Scholtz, "Comparisons of analog and digital impulse radio for multiple-access communications," in Proc. IEEE Int. Conf. on Communication., June 1997, vol. 1, pp. 91-95, Montreal, Canada.

2. J. Foerster, E. Green, S. Somayazulu, D. Leeper, "Ultra-Wideband Technology for Short- or Medium-Range Wireless Communications", Intel Technology Journal Q2, 2001.

3. M. Z. Win, "On the power spectral density of digital pulse streams generated by M-ary cyclostationary sequences in the presence of stationary timing jitter," IEEE Tran. on Commun., vol. 46, no. 9, pp. 1135-1145, Sep. 1998.

4. M. Z. Win, "Spectral Density of Random Time-Hopping Spread-Spectrum UWB Signals with Uniform Timing Jitter", Proc. MICOM '99, vol. 2, pp. 1196-1200, 1999.

5. M. Z. Win and R. A. Scholtz, "Ultra-Wide Bandwidth Time-Hopping Spread-Spectrum Impulse Radio for wireless multiple-access communications", IEEE Transaction on Communications, vol. 48, no. 4, pp. 679-691, Apr. 2000.

6. S. Mo, A. D. Gelman and J. Gopal, "Frame Synchronization in UWB Using Multiple SYNC Words to Eliminate Line Frequencies", in Proc. IEEE Wireless Communications and Networking Conference, March 2003, New Orleans, LA.

7. S. Mo and A. D. Gelman, "Base-band Data Whitening to Minimize Power Spectral Density of Multi-band UWB Signals", internal report of Panasonic Information and Networking Technologies Lab, April 2003.

8. S. Mo and A. D. Gelman, "Scrambler Design to Reduce Power Spectral Density of UWB Signals in IEEE 802.15.3a", internal report of Panasonic Information and Networking Technologies Lab, October 2003

9. Infineon Tech., "Synchronous Simultaneous Operating Piconets," IEEE 802.15 Working Group for Wireless Personal Area Network (WPANs), Sept. 2003.

10. L. R. Welch, "Lower Bounds on the Maximum Cross Correlation of Signals of Signals," IEEE Trans. on Information Theory, vol. IT-20, pp.397-399, May 1974.

11. J. L. Massey and T. Mittelholzer, "Welsh's Bound and Sequence Sets for Code-Divison Multiple-Access Systems," in Sequences II : Methods in Communication, Security and Computer Science, R. Capocelli, A.D.Santis, and U. Vaccaro, Eds. New York: Springer-Verlag, 1991.

12. S. Ulukus and R. Yates, "Iterative construction of optimum signature sequence sets in synchronous CDMA systems,"IEEE Transaction on Information Theory, vol. 47, pp.1989-1998, July, 2001.

13. C. Rose, S. Ulukus and R.Yates, " Interference Avoidance for Wireless Systems," in Proc. Vehicular Technology Conf., vol. 2, Tokyo, Japan, 2000, pp. 901-906.

14. P. Vishwanath and V.Anantharam, "Optimal Sequences and Sum Capacity of synchronous CDMA systems," IEEE Transaction on Information Theory, vol. 45, pp. 1984-1991, Sept. 1999.

15. S. Haykins, Communication Systems (4/e), John Wiley and Sons, 2001.

16. J. S. Goldstein, I. S. Reed, L. L. Scharf, "A Multi-Stage Representation of the Weiner Filter Based on Orthogonal Projections," IEEE Transaction on Information Theory, vol. 44, no. 7, Nov. 1998.

17. S. Haykins, Adaptive Filter Theory (3/e), Prentice Hall, 1991.

18. A. H. Tewfik, " Multicarrier UWB," 03147r3P802-15_TG3a, May2003.

19. FCC. "Revision of part 15 of the commission's rules regarding Ultrawideband transmission systems". First Report and Order, ET Docket 98-153, April 2002.

20. G. F. Ross, "The transient analys of multiple beam feed networks for array systems," PhD thesis, Polytechnic Institute of Brooklyn, 1963.

21. B. Mielczarek, M. Wessman, and A. Svensson, "Performance of coherent UWB Rake receivers with channel estimators," Proceedings IEEE Vehicular Techonology Conference Fall, October 2003.

22. P. Gandolfo, "TG3 Coexistence capabilities," IEEE 802.15-02/157r0. March, 2002.

23. E. Fujita, et al., "Sony CFP Presentation," IEEE P802.15-03/137r3, May 2003.

24. M. McLaughlin, et al., "The ParthusCeva UltraWideband PHY Proposal," IEEE P802.15-03/123r3, May 2003.

25. A. W. Marshall and I. Olkin, Inequalities: Theory of Majorization and Its Applications. New York: Academic, 1979.

26. J. G. Proakis and M. Salehi, Communication Systems Engineering (2/e), Prentice Hall, 2001.